Systems/Circuits

Relating Pupil Diameter and Blinking to Cortical Activity and Hemodynamics across Arousal States

Kevin L. Turner,[1,2] Kyle W. Gheres,[2,3] and Patrick J. Drew[1,2,3,4]

[1]Department of Biomedical Engineering, Pennsylvania State University, University Park, Pennsylvania 16802, [2]Center for Neural Engineering, Pennsylvania State University, University Park, Pennsylvania 16802, [3]Departments of Engineering Science and Mechanics, and [4]Biology and Neurosurgery, Pennsylvania State University, University Park, Pennsylvania 16802

Arousal state affects neural activity and vascular dynamics in the cortex, with sleep associated with large changes in the local field potential and increases in cortical blood flow. We investigated the relationship between pupil diameter and blink rate with neural activity and blood volume in the somatosensory cortex in male and female unanesthetized, head-fixed mice. We monitored these variables while the mice were awake, during periods of rapid eye movement (REM), and non-rapid eye movement (NREM) sleep. Pupil diameter was smaller during sleep than in the awake state. Changes in pupil diameter were coherent with both gamma-band power and blood volume in the somatosensory cortex, but the strength and sign of this relationship varied with arousal state. We observed a strong negative correlation between pupil diameter and both gamma-band power and blood volume during periods of awake rest and NREM sleep, although the correlations between pupil diameter and these signals became positive during periods of alertness, active whisking, and REM. Blinking was associated with increases in arousal and decreases in blood volume when the mouse was asleep. Bilateral coherence in gamma-band power and in blood volume dropped following awake blinking, indicating a reset of neural and vascular activity. Using only eye metrics (pupil diameter and eye motion), we could determine the arousal state of the mouse ('Awake,' 'NREM,' 'REM') with >90% accuracy with a 5 s resolution. There is a strong relationship between pupil diameter and hemodynamics signals in mice, reflecting the pronounced effects of arousal on cerebrovascular dynamics.

Key words: **blinking; hemodynamics; local field potential; neurovascular coupling; pupil; sleep scoring**

Significance Statement

Determining arousal state is a critical component of any neuroscience experiment. Pupil diameter and blinking are influenced by arousal state, as are hemodynamics signals in the cortex. We investigated the relationship between cortical hemodynamics and pupil diameter and found that pupil diameter was strongly related to the blood volume in the cortex. Mice were more likely to be awake after blinking than before, and blinking resets neural activity. Pupil diameter and eye motion can be used as a reliable, noninvasive indicator of arousal state. As mice transition from wake to sleep and back again over a timescale of seconds, monitoring pupil diameter and eye motion permits the noninvasive detection of sleep events during behavioral or resting-state experiments.

Introduction

The dynamics of the eyes convey information about mental state. In addition to their respective roles in controlling light levels and protecting the eye, pupil diameter and blinking give information about the state of neural activity in the brain (Strauch et al., 2022). However, for measures of pupil diameter and blinking to be useful, we must understand their relationship to neural and vascular physiology. Pupil dilations are associated with higher levels of arousal during the awake state (Hess and Polt, 1964; Kahneman and Beatty, 1966; Yoss et al., 1970; Morad et al., 2000; Drew et al., 2001; Onorati et al., 2013) and correlate with increased sympathetic activity (Bradley et al., 2008). The pupil will usually dilate when a subject is performing a task or making a decision (Hakerem and Sutton, 1966; Einhäuser et al., 2010; Gilzenrat et al., 2010; Nassar et al., 2012; Burlingham et al., 2022), and recent rodent work has shown that pupil diameter fluctuations temporally track cortical state (Reimer et al., 2014; McGinley et al., 2015; Vinck et al., 2015). In both rodents and primates, pupil dilation reflects noradrenergic tone in the cortex as well as activity in the locus ceruleus (LC; Preuschoff et

Received June 24, 2022; revised Dec. 6, 2022; accepted Dec. 9, 2022.

Author contributions: K.L.T. and P.J.D. designed research; K.L.T. performed research; K.L.T. and K.W.G. contributed unpublished reagents/analytic tools; K.L.T. analyzed data; K.L.T. and P.J.D. wrote the paper.

This work was supported by National Institutes of Health–National Institute of Neurological Disorders and Stroke Grants R01NS078168 and R01NS079737 to P.J.D. We thank Nikki Crowley for comments and feedback on the manuscript.

The authors declare no competing financial interests.

Correspondence should be addressed to Patrick J. Drew at pjd17@psu.edu.

https://doi.org/10.1523/JNEUROSCI.1244-22.2022

al., 2011; Joshi et al., 2016; Reimer et al., 2016; Larsen and Waters, 2018). In addition to its effects on neurons, noradrenergic input from the LC causes vasoconstriction of cortical arteries (Bekar et al., 2012). LC activity and noradrenergic tone provides a potential mechanism for coupling arousal to cortical hemodynamics (Pisauro et al., 2016), as changes in pupil diameter are also correlated with blood-oxygen-level-dependent (BOLD) signals seen in neuromodulatory centers during functional magnetic resonance imaging (fMRI; Pais-Roldan et al., 2020; Sobczak et al., 2021). Both head-fixed and freely behaving mice frequently sleep with their eyes open (Yüzgeç et al., 2018; Karimi Abadchi et al., 2020; Turner et al., 2020; Senzai and Scanziani, 2022). Pupil diameter decreases during sleep and can be used to detect sleep events on a minute-to-minute timescale (Yüzgeç et al., 2018; Karimi Abadchi et al., 2020), making it a particularly useful metric for attention and behavioral monitoring.

Blink rate is influenced by mental state and fatigue (Holland and Tarlow, 1972; Stern et al., 1994; Nakamori et al., 1997; Van Orden et al., 2001). Humans blink every few seconds (Stern et al., 1984), although blinking is less frequent in rodents (Kaminer et al., 2011). Blink rate is modulated by dopaminergic tone (Karson, 1983) and is higher in individuals with schizophrenia (Karson, 1979; Karson et al., 1990). Blinking causes brief decreases in neural activity in visual areas that are similar to transient darkening (Gawne and Martin, 2000; Golan et al., 2016). However, blinking also drives BOLD signals in the visual cortex (Bristow et al., 2005a,b; Hupé et al., 2012) and somatosensory regions (Guipponi et al., 2015), and blinks are correlated with BOLD activity in the default mode network (Nakano et al., 2013). Blinking is correlated with changes in neural and vascular dynamics across the brain, although the correlates of blinking with arousal are not as well understood.

To better understand how pupil diameter and blinking relate to neural activity and cortical hemodynamics across arousal states, we analyzed videos of the eye with concurrent monitoring of neural activity and blood volume in the somatosensory cortex of head-fixed mice of both sexes. We investigated the relationship between spontaneous changes in pupil diameter and these physiological signals during the awake state, as well as during rapid eye movement (REM) and non-rapid eye movement (NREM) sleep. We also tracked how neural activity and cortical blood volume changed around blinking events. Using only changes in pupil diameter and eye position, we found that we can accurately detect and categorize REM and NREM sleep events on a timescale of seconds, providing a simple and robust measure of arousal for studies using eye monitoring in rodents.

Materials and Methods

Data presented here are from 22 C57BL/6J mice (12 males between the ages of 3 and 8 months; The Jackson Laboratory). Data from 14 of these mice were previously published (Turner et al., 2020), and we have added imaging/recordings from an additional eight mice. We obtained a total of 442.75 h of data (20.1 ± 5.3 h per mouse) of naturally occurring 'Awake' (61.4 ± 17.3%), 'NREM' sleep (34.2 ± 16.1%), and 'REM' sleep (4.4 ± 2.8%) data.

Arousal state nomenclature. Capitalized italics (*Rest*, *NREM*, *REM*, *Alert*, *Asleep*, and *All*) denote arousal states with specific inclusion criteria. Capitalized nonitalics with single quotes refer to individual 5 s labels of arousal state classified using a machine learning algorithm ('Awake,' 'NREM,' 'REM'), and we use the term 'Asleep' (nonitalicized) to refer to events classifications as either 'NREM' or 'REM' (see Figs. 4, 5). When generally discussing arousal state in all other contexts, we use the terms awake, sleep, NREM sleep, REM sleep, and so on with no italics or other indicators.

Animal procedures. This study was performed in accordance with the recommendations of the *Guide for the Care and Use of Laboratory Animals* of the National Institutes of Health. All procedures were performed in accordance with protocols approved by the Institutional Animal Care and Use Committee of Pennsylvania State University (Protocol no. 201042827). A head bar, as well as cortical, hippocampal, and nuchal muscle electrodes along with bilateral polished and reinforced thinned-skull windows (Drew et al., 2010; Shih et al., 2012; Zhang et al., 2022b) were surgically implanted under isoflurane anesthesia (5% induction, 2% maintenance). Detailed surgical procedures have been previously described (Winder et al., 2017; Turner et al., 2020; Mirg et al., 2022a,b). Following surgery, animals were housed individually on a 12 h light/dark cycle (lights on at 7:00 A.M.) with food and water *ad libitum*. Each animal was gradually acclimated to head fixation in the weeks following recovery. Following the conclusion of imaging experiments, animals were deeply anesthetized and transcardially perfused with heparin-saline followed by 4% paraformaldehyde for histologic verification of electrode placement (Drew and Feldman, 2009; Adams et al., 2018).

Physiologic data acquisition. Data were acquired with a custom LabVIEW program (National Instruments; https://github.com/DrewLab/LabVIEW-DAQ). For details on intrinsic optical signal (IOS) imaging, electromyography (EMG), electrophysiology, whisker stimulation, and behavioral measurements (Turner et al., 2020; Zhang et al., 2022b). Previous work from our lab has shown that the intrinsic signal is not affected by skull/brain movement or other motion artifacts. In previously published experiments (Winder et al., 2017), we looked at reflectance changes in a piece of clay mounted over the cranial window, which would be sensitive to any motion artifacts as well as any other nonhemodynamic noise sources. The reflectance changes were on the order of 0.01%, much smaller than the ~20% changes in reflectance (ΔR/R) we see during sleep. Furthermore, two-photon imaging from our lab of mice running on a treadmill (Gao and Drew, 2014; Echagarruga et al., 2020) showed ~2 μm of brain/skull motion during locomotion (a more extreme imaging condition than presented here), which is too small to have an impact on the IOS. IOS reflectance was converted to changes in total hemoglobin (Δ[HbT]) using the Beer–Lambert law (Ma et al., 2016a, b). Data were acquired in 15 min intervals with a <1 min gap in between for saving data to disk. The vibrissae (left, right, or a third air puffer not directed at the body as an auditory control) were randomly stimulated with air puffs [0.1 s, 10 pounds force per square inch (PSI)] occurring every 30–45 s for the first ~1 h of imaging.

Pupil diameter measurement. The pupil was illuminated with 780 nm light measured at 0.02–0.05 mW/mm^2 on a Standard Photodiode Power Sensor (catalog #S120VC, Thorlabs) as mice are functionally blind to these wavelengths (Breuninger et al., 2011; Chang et al., 2013). To prevent constriction of the pupil by the illumination for IOS, a dichroic mirror located above the head was used to block as much of the IOS illumination from the eyes as possible so that the mouse was only exposed to a faint glow in its periphery (0.002–0.005 mW/mm^2) with no visible wavelength light shining directly into its eyes. We did not try to eliminate all green light reaching the eye because green light has sleep-promoting effects (Pilorz et al., 2016). However, we did not quantify the pupil diameter in complete darkness as higher baseline dilations would result in the pupil edges being obscured by the eyelid. All pupil diameter measurements were verified by manual inspection (K.L.T.).

Automated pupil diameter measurement and blink detection. Pupil diameter was extracted from videos of the eye taken using a Basler GigE ace acA640-120gm camera with a 75 mm double Gauss, fixed focal length lens (catalog #54-691, Edmond Optics) at 30 frames/s. Our pupil detection algorithm was adapted from the thresholding in Radon space (TiRS) algorithm developed to determine vessel cross sections (Gao and Drew, 2014). The sclera and pupil were defined as the area within a user-selected region of interest (ROI) created by outlining the first frame with the eye fully open. Images were inverted so that the pupil had the maximal intensity and were 2-D median filtered [(5,5) *x*, *y* pixel median]. The

pixel intensity distribution was fit with a normal distribution using maximum likelihood estimation (MLE), and pixels above a user-defined threshold (average of 1 ± 0.25 SDs from the MLE mean) were set to one, and all other pixel intensities were set to zero. The binarized image was then converted to Radon space and normalized within each projection angle (Gao and Drew, 2014). A second threshold was applied before conversion back to image space, and any holes within the filtered pupil object were filled. Framewise pupil area was then calculated using a boundary classification algorithm. Occasional obstructions of the pupil (by a vibrissae) were identified by detecting rapid fluctuations in pupil area. For these frames, the threshold used for thresholding in Radon space was iteratively decreased until the pixel area was within framewise change boundaries. Any periods where the pupil was obscured or otherwise unmeasurable were discarded from analysis. The TiRS algorithm was developed to detect small changes in the area of an ellipse (Gao and Drew, 2014). Other techniques, including using a deep neural network such as DeepLabCut (Mathis et al., 2018), can be used to track the pupil diameter and position as well (Privitera et al., 2020), although this requires training the network. Although the pupil was slightly elliptical in appearance because of the angle of the camera and movement of the eye, the correlation between the major and minor axis of the area of the object was 0.96 ± 0.02 ($N = 22$ mice), indicating the ellipse at the pupil boundary does not appreciably change shape, only size. The area (A) was used to calculate the diameter (d) of the pupil using the formula $d = 2\sqrt{A/\pi}$. The following MATLAB functions were used: roipoly, medfilt2, imcomplement, mle, pdf, radon, iradon, bwboundaries, bwconvhull, imfill, regionprops, diff, fillmissing.

Blink detection. Blinking was detected independently of pupil diameter from the same ROI as used for pupil diameter measurements. Rapid changes in eyelid motion were detected by using the sum of pixel intensities within the user-defined ROI. The intensity of all pixels for each frame (sclera and pupil) were summed, and a frame-to-frame ROI intensity difference was calculated. As the eyelid obscures the pupil during blinks, rapid changes in overall pixel intensity corresponded to eyelid movements. A threshold was applied to binarize changes in luminance across frames, and blinking events were extracted as above thresholded changes in image intensity. As mice frequently blinked several times in rapid succession, blinking events that occurred with <1 s between them were concatenated into a single blinking bout. Periods where a false-positive blink was detected, such as from the eye only partially closing, were also discarded. All detected blinking events were verified by manual inspection (K.L.T.).

Electrophysiological analysis. Discrete LFP bands were digitally bandpass filtered from the broadband data using a third-order Butterworth filter into the following bands: delta [1–4 Hz], theta [4–10 Hz], alpha [10–13 Hz], beta [13–30 Hz], and gamma [30–100 Hz]. The filtered signal was then squared, low-pass filtered <10 Hz, and resampled at 30 Hz. Time-frequency spectrograms were calculated using the Chronux toolbox version 2.12 v03 (Bokil et al., 2010), function mtspecgramc with a 5 s window and 1/5 s step size using [5,9] tapers and a passband of 1–100 Hz to encompass the LFP. EMG (300–3 kHz) from the nuchal (neck) muscles was bandpass filtered, squared, convolved with a Gaussian kernel with 0.5 s SD, log transformed, and then resampled at 30 Hz. MATLAB functions used were butter, zp2sos, filtfilt, gausswin, log10, conv, resample.

Sleep scoring. Sleep states were scored consistent with previously published criteria (Cirelli, 2009; Weber and Dan, 2016; Saper and Fuller, 2017). NREM sleep is marked by predominantly elevated cortical delta-band power and lower EMG power during slow-wave (REM sleep; Steriade et al., 1993; Amzica and Steriade, 1998). REM sleep is marked by elevated hippocampal theta-band power and elevated cortical gamma-band power with even further reduced EMG power (muscle atonia; Cantero et al., 2004; Montgomery et al., 2008; Le Van Quyen et al., 2010; Sullivan et al., 2014). Periods of user-verified awake rest >5 s in duration with no whisker stimulation, no whisker motion, and no detectable body motion were identified and used baseline characterization of all signals as well as for z-scoring the pupil. Sleep scoring was performed as in Turner et al. (2020). Every 5 s interval was classified as either Awake, NREM sleep, or REM sleep using a bootstrap aggregating random forest model with the predictors of cortical delta FP, cortical beta LFP, cortical gamma LFP, hippocampal theta LFP, EMG power, heart rate, and whisking duration. Sleep model accuracy was validated using the out-of-bag error during model training. MATLAB functions used were TreeBagger, oobError, predict.

Pupil diameter during different arousal states. Pupil diameter was taken from awake resting events (*Rest*, ≥10 s in duration), volitional whisking (*Whisk*, 2–5 s), whisker stimulation (*Stim*, 0.1 s, 10 PSI to vibrissa), *NREM* (≥30 s), and *REM* (≥60 s). Pupil diameter was low-pass filtered <1 Hz with a fourth-order Butterworth filter. Changes in whisking-evoked and stimulus-evoked (contralateral, auditory) diameters were taken as the change in diameter relative to the mean of the 2 s preceding the event onset. Classifications of *Alert* or *Asleep* were taken as 15 min periods with no whisker stimulation and at least 80% of a given classification (Awake for *Alert*, NREM or REM for *Asleep*) within a 15 min recording. The classification of *All* denotes all data taken during periods with no sensory stimulation, independent of arousal state. MATLAB functions used were butter, zp2sos, filtfilt.

Power spectra and coherence. Spectral power was estimated using the Chronux toolbox (Bokil et al., 2010) function mtspectrumc. For prewhitening spectra, the first derivative was taken of the mean-subtracted data before the power calculation. Gamma-band power measurements were scaled by a factor of 1×10^{19} so that the magnitude of the neural changes [arbitrary units (a.u.)] were more in line with those from the hemodynamic signal for ease of comparison. Coherence analysis was run for each data type using the Chronux function coherencyc with MATLAB functions detrend and diff.

Δ[HbT]/Gamma-band power versus pupil relationship. Mean changes in total hemoglobin (Δ[HbT]) or gamma-band power (ΔP/P), and pupil diameter (z-units) during each arousal state classification ('Awake,' 'NREM,' 'REM') was plotted as a 2D histogram to highlight clustering in each class. Each classification was assigned a color, and the three images were merged as a composite in Fiji (ImageJ) software. MATLAB function used was histogram2.

Cross-correlation. Data were low-pass filtered <1 Hz using a fourth-order Butterworth filter and mean subtracted. Cross-correlation analysis was run for each arousal state with either a ± 5 s lag (*Rest*, *NREM*, *REM*) or ± 30 s lag (*Alert*, *Asleep*, *All*) depending on duration of the behavioral state. MATLAB functions used were xcorr, filtfilt, and detrend.

Interblink interval and blink-associated physiology. Because of gaps in recording to save the data to disk, interblink interval was calculated between blinks occurring within 15 min records and not blinks on the edges of trials. Blinks that occurred within 1 s of each other were linked together as blinking bouts, and all blink-triggered analyses were with respect to the first blink in a series. Blink-triggered averages were separated into two groups depending on the arousal state classification of the 5 s bin before the blink, being either Awake (arousal state classification of Awake) or Asleep (arousal state classification being either NREM or REM).

Probability of sleep as a function of pupil diameter. The probability of being in each arousal state ('Awake,' 'NREM,' 'REM') as a function of pupil diameter was obtained from the mean diameter during each 5 s sleep score and binning the value into a histogram, which was then smoothed with a median filter and Savitzky–Golay filter. MATLAB functions used were medfilt1 and sgolayfilt.

Tracking of pupil location. Motion of the pupil was tracked by using the X and Y coordinates of the centroid obtained during pupil tracking and comparing the change in position to the baseline position during *Rest*. Frame-by-frame changes in centroid location were low-pass filtered <10 Hz using a fourth-order Butterworth filter. Motion of the eye was evaluated during each arousal state classification (Awake, NREM, REM) by taking the cumulative sum of the absolute change in centroid position within each 5 s bin. Transitions between among states ('Awake,' 'NREM,' 'REM') for pupil diameter, position, and motion were extracted from arousal classifications with 30 s of consecutive classifications of one state followed by 30 s of another.

Eye, Physiological, and Combined model comparison. The Eye Model was trained using only eye metrics, pupil diameter (mean, variance, minimum of both z-unit and mm diameter), position (mean, variance, and

maximum displacement of the *x*, *y* centroid), and motion (sum, variance of the absolute velocity of the centroid) from data with open eyes. The Physiological Model was trained using non-eye-based measures (cortical delta power, hippocampal theta power, EMG, and so on (Turner et al., 2020) from the same data so that the training/testing sets were identical among models. The Combined Model used a union of all parameters from both models. Each model used was trained using a bagged random forest composed of 128 decision trees, with out-of-bag error and confusion matrices from each animal being calculated at the time of model training using a 70–30 (training/testing) split of randomly shuffled labels taken from each arousal state. MATLAB functions used were TreeBagger, oobError, predict, and confusionchart.

Experimental design and statistical analysis. Researchers were not blind to the experimental conditions or data analysis. Sample sizes are consistent with those of previously published studies (Huo et al., 2015; Winder et al., 2017; Echagarruga et al., 2020; Turner et al., 2020). Statistical evaluations were made using either generalized linear mixed-effects (GLME) models with the arousal state as a fixed effect, mouse identity as a random effect, and hemisphere [left/right (L/R), if applicable] as an interaction with the animal ID, or using a paired *t* test where appropriate. Unless otherwise stated, statistical results report *p* values from a GLME test. All reported quantifications are mean ± SD unless otherwise indicated. Unless otherwise noted, all pupil diameter measurements are in *z*-units. MATLAB functions used were fitglme, *t* test.

Data availability. Data and sample files for running the pupil tracking algorithm are available at doi:10.5061/dryad.05qfttf5w and analysis code is available at https://github.com/DrewLab/Turner-JNeurosci2022. Data were analyzed with code written by K.L.T, K.W.G, and P.J.D. (MATLAB 2019b–2022a, MathWorks,).

Results

Unanesthetized mice were head fixed under an IOS imaging setup (Sirotin and Das, 2009; Pisauro et al., 2013; Huo et al., 2014; Vazquez et al., 2014; Winder et al., 2017) with concurrent electrophysiology to measure changes in neural activity from the vibrissa region of the somatosensory cortex (Petersen, 2007, 2014) and hippocampal CA1. We also tracked whisker motion (Winder et al., 2017), electromyography of the nuchal muscles (Turner et al., 2020), and pupil diameter/blinking (Reimer et al., 2014; Vinck et al., 2015; Reimer et al., 2016; Larsen and Waters, 2018; Fig. 1*a*). Using the thresholding in Radon space algorithm (Gao and Drew, 2014), we detected the outline of pupil from video frames (Fig. 1*b–e*, Movie 1) to quantify diameter changes. Blinks were detected from rapid pupil diameter changes (Fig. 1*f*). During the awake state, there are frequent bouts of whisker motion that are correlated with increases in pupil diameter, and the EMG has high power. The LFP has reduced low-frequency power, and hemodynamic fluctuations have low amplitude, except during periods of extended behavior or sensory stimulation. During NREM sleep, whisker motion and EMG power are much lower, and the pupil diameter is smaller than in the awake state. Cortical LFP and hemodynamic signals both begin to increase in amplitude with low-frequency oscillations in broadband LFP power. During REM sleep, whisker motion increases along with eye movement, but the pupil remains constricted. Power in the EMG is at its lowest point because of muscle atonia (with occasional twitches), blood volume increases substantially above both awake and NREM levels (Bergel et al., 2018), and a prominent theta band is visible in the hippocampal LFP. A representative example of how pupil diameter changes along with fluctuations in Δ[HbT], hippocampal LFP, and other behavioral cues during each arousal state is shown in Figure 1*f* and Movie 1. As mice have been shown to sleep with their eyes open during both head-fixed (Yüzgeç et al., 2018; Karimi Abadchi et al., 2020; Turner et al., 2020) and freely moving (Senzai and Scanziani, 2022) conditions, we tested whether neural activity and hemodynamics might differ between the eyes-open and eyes-closed instances of the REM state. We compared the eyes-open REM sleep physiology with that obtained during a few instances of REM sleep with eyes closed in a subset of mice ($N = 8$), which was excluded from subsequent analyses because of the inability to measure pupil diameter. The change in total hemoglobin (Δ[HbT]) during REM with eyes open (73.9 ± 12.9 μM) was not significantly different from the hemoglobin changes during REM sleep with eyes closed (76.2 ± 21.2 μM, $p = 0.49$, paired *t* test). The difference in theta band power in the hippocampus during eyes-open REM and eyes-closed REM was also not statistically significant (1.06 ± 1.11 a.u. vs 1.06 ± 1.10 a.u., respectively; $p = 0.96$, paired *t* test). The lack of detectable difference between the eyes-open and eyes-closed sleep state suggests that whether or not eyes are open has little impact on sleep physiology.

Quantification of pupil diameter across arousal states

To quantify how fluctuations in pupil diameter change with arousal state, we compared the diameter of the pupil during several distinct arousal states and behaviors. Pupil diameter was largest during periods of arousal and smallest during sleep. To standardize measures across animals and to account for slight differences in baseline illumination intensity, we *z*-scored the pupil diameter to the mean and SD during all periods of awake quiescence lasting at least 5 s in length. Italics denote periods meeting our arousal state criteria. Fifteen-minute periods with at least 80% of its model scores as 'Awake' were classified as *Alert*; and 15 min periods with 80% of the time in 'NREM' or 'REM' sleep were classified as *Asleep*. *All* was all data, regardless of arousal state. Periods with whisker stimulation were excluded from all states. Two mice did not have any 15 min periods that met the criteria for the *Alert* or *Asleep* categories ($N = 20$ mice included) with the other four behaviors (*Rest, NREM, REM, All)* all having $N = 22$ mice. *Rest,* defined as all periods of awake quiescence lasting at least 10 s in length, had a mean pupil diameter of 0.6 ± 0.17 mm (Fig. 2*a*) or −0.25 ± 0.88 *z*-units (Fig. 2*b*). We used a GLME model to compare the diameter of the pupil among states, using the Bonferroni correction for multiple comparisons (10), which puts the adjusted significance threshold (α) at 0.005. The mean *z*-unit during *Rest* was nonzero because the minimum duration used for *z*-scoring (5 s) was shorter than the minimum duration for inclusion in *Rest* (10 s). During volitional whisking bouts lasting 2–5 s, pupil diameter increased to 0.89 ± 0.17 mm ($p = 2.3 \times 10^{-19}$ vs *Rest*) or 3.39 ± 0.88 *z*-units ($p = 2.1 \times 10^{-22}$). Following brief stimulation of the vibrissae, pupil diameter increased to 0.75 ± 0.18 mm ($p = 9.2 \times 10^{-8}$) or 1.95 ± 1.82 *z*-units ($p = 1.9 \times 10^{-11}$). The pupil diameter decreased during *NREM* (>30 s in length) to 0.35 ± 0.07 mm ($p = 8.1 \times 10^{-16}$) or −3.43 ± 0.64 *z*-units ($p = 6.2 \times 10^{-19}$) and even further during *REM* (>60 s in length) to 0.26 ± 0.03 mm ($p = 3.2 \times 10^{-23}$) or −4.56 ± 0.75 *z*-units ($p = 2.3 \times 10^{-27}$). Additional statistical comparisons for the difference in pupil size between each arousal state can be found in Tables 1 and 2. Periods of volitional whisking and whisker stimulation caused increases in pupil diameter of 1.44 ± 0.47 *z*-units and 1.61 ± 0.62 *z*-units, respectively. Auditory controls dilated the pupil by 0.98 ± 0.58 *z*-units (Fig. 2*c*). Note that although the *z*-unit diameter was set relative to awake resting events, these increases are with respect to changes in *z*-unit diameter relative to the 2 s before event onset, which was a mixture of awake resting and volitional behaving data of various durations.

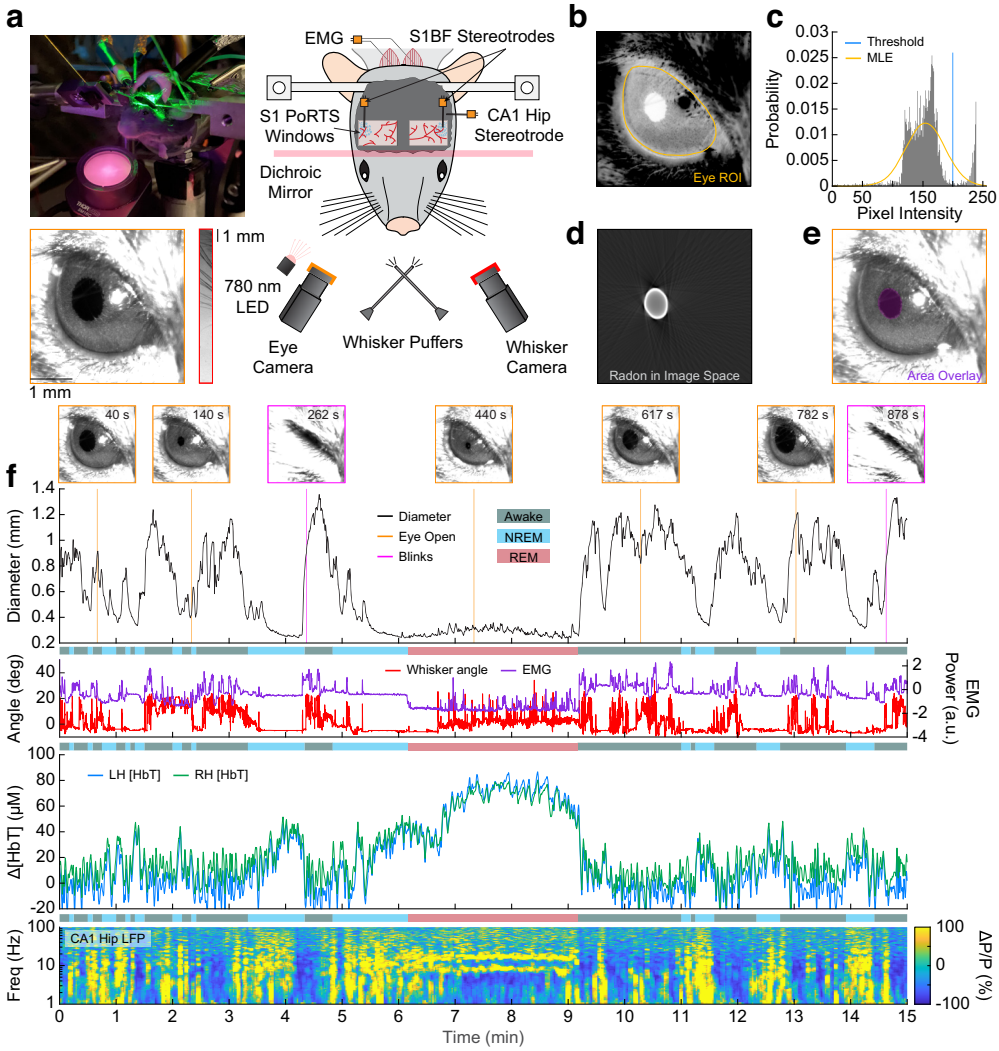

Figure 1. Pupil diameter tracks arousal state. ***a***, Photograph and schematic of the experimental setup. IOS imaging of the whisker portion of somatosensory cortex collected using illumination at an isosbestic point of hemoglobin (530 or 568 nm) through bilateral polished and reinforced thinned-skull windows (PoRTS). Electrodes were implanted into layer 5 of the somatosensory cortex and into hippocampal CA1. EMG electrodes were also implanted into the nuchal muscles of the neck. A camera is directed toward the whiskers to track their movement. Another camera captures the eye, which is illuminated by infrared 780 nm light, to observe pupil diameter and blinking. Directed air puffers allow controlled stimulation of the left and right whiskers. ***b***, ROI around the mouse eye. ***c***, Histogram of pixel intensities in the ROI showing separation between the intensities in the pupil and sclera. A threshold (blue) is set for initial diameter estimation based on an MLE of the sclera intensity (orange). ***d***, Image of the pupil after it has been thresholded in Radon space and transformed back into image space. ***e***, Detected pupil superimposed on video frame. ***f***, Example showing changes in pupil diameter, whisker angle [deg], EMG power [arbitrary units, a.u.], Δ[HbT], and power changes (ΔP/P) in the CA1 LFP during awake, NREM, and REM periods.

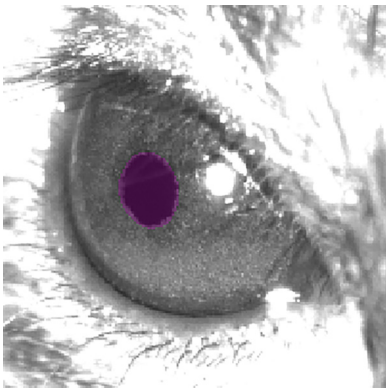

Movie 1. Video showing pupil diameter variations across several arousal states. Detected pupil area is in purple. [View online]

To look at changes in the power spectrum of the pupil diameter during different arousal states, we prewhitened the pupil diameter throughout analysis during periods of continuous *Rest* (>10 s duration), continuous *NREM* (>30 s duration), continuous *REM* (>60 s duration), and three additional longer-length classifications (*Alert*, *Asleep*, and *All*) by taking the first temporal derivative of the *z*-unit diameter before power estimation. Except for *REM*, the prewhitened power spectra of the pupil diameter during the longer length behaviors were similar to each other at the lower frequencies (Fig. 2*d*). These findings support previous reports that the pupil diameter increases with arousal but decreases during periods of sleep (Yüzgeç et al., 2018; Karimi Abadchi et al., 2020).

Relationship between pupil diameter and hemodynamic and neural signals

We next asked how well the pupil diameter correlated with both hemodynamic and neural signals in the somatosensory cortex of mice both during awake behaviors and during different sleep

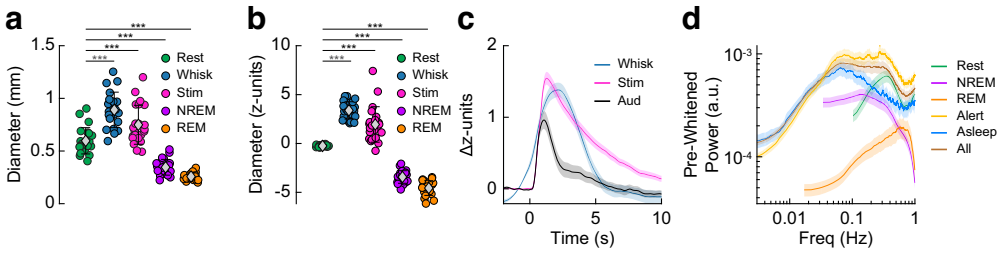

Figure 2. Quantification of pupil diameter across arousal states. ***a***, Mean pupil diameter (mm) for each arousal state. Mean of each animal is a circle. Gray diamond and error bars indicate mean ± SD across animals for each arousal state. ***b***, Mean pupil diameter (*z*-units) for each arousal state. ***c***, Whisking-evoked and stimulus-evoked increases in pupil diameter based on the 2 s before event onset. ***d***, Prewhitened power spectrum of pupil diameter (*z*-units) during different arousal states. Shading (***c***, ***d***) indicate SEM. Error bars (***a***, ***b***) indicate SD. Statistical comparisons shown are between *Rest* and other states using a GLME model with Bonferroni correction for multiple comparisons (10) $^{*}\alpha < 0.005$, $^{**}\alpha < 0.001$, $^{***}\alpha < 0.0001$. Tables 1 and 2 provide additional statistical comparisons between each arousal state in ***a***, ***b***.

Table 1. Statistical comparison of mean pupil diameter across arousal states (mm)

	Rest	Whisk	Stim	NREM	REM
Rest		***2.3 × 10–19	***9.2 × 10–8	***8.1 × 10–16	***3.2 × 10–23
Whisk	***2.3 × 10–19		***5.4 × 10–7	***1.2 × 10–38	***2.8 × 10–44
Stim	***9.2 × 10–8	***5.4 × 10–7		***2.3 × 10–28	***6.0 × 10–35
NREM	***8.1 × 10–16	***1.2 × 10–38	***2.3 × 10–28		*0.0012
REM	***3.2 × 10–23	***2.8 × 10–44	***6.0 × 10–35	*0.0012	

Bonferroni-corrected significance levels (10), $^{*}\alpha < 0.005$, $^{**}\alpha < 0.001$, $^{***}\alpha < 0.0001$.

Table 2. Statistical comparison of mean pupil diameter across arousal states (*z*-units)

	Rest	Whisk	Stim	NREM	REM
Rest		***2.1 × 10–22	***1.9 × 10–11	***6.2 × 10–19	***2.3 × 10–27
Whisk	***2.1 × 10–22		***3.1 × 10–6	***2.3 × 10–43	***2.2 × 10–49
Stim	***1.9 × 10–11	***3.1 × 10–6		***1.2 × 10–34	***1.3 × 10–41
NREM	***6.2 × 10–19	***2.3 × 10–43	***1.2 × 10–34		**0.00019
REM	***2.3 × 10–27	***2.2 × 10–49	***1.3 × 10–41	**0.00019	

Bonferroni-corrected significance levels (10), $^{*}\alpha < 0.005$, $^{**}\alpha < 0.001$, $^{***}\alpha < 0.0001$.

states. For each mouse, the pupil diameter was compared with both the neural and hemodynamic signals of the hemispheres, yielding 2 * *N* measurements for each behavior. The nonindependence (because of within-animal correlations) was accounted for as an interaction term in the statistical comparison (see above, Materials and Methods). During the 'Awake' state, changes in pupil diameter and gamma-band power were small. When the animals were in 'REM' and 'NREM' sleep, the pupil constricted and gamma-band power increased substantially relative to the 'Awake' state (Fig. 3*a*). We then looked at the coherence and the cross-correlation between the envelope of gamma-band power (ΔP/P) and pupil diameter. The minimum cross-correlation during *Rest* was −0.16 ± 0.20 at a lag of −0.07 s (Fig. 3*b*) and during *Alert* was −0.02 ± 0.14 at 0.1 s (Fig. 3*c*), indicating very little time difference between cortical gamma-band and corresponding pupil diameter fluctuations during awake behaviors. Extrema in the cross-correlation in *NREM* were −0.26 ± 0.06 at −0.1 s; *REM*, 0.05 ± 0.04 at 1.53 s; *Asleep*, −0.32 ± 0.05 at −0.43 s; and *All*, −0.23 ± 0.11 at −0.2 s.

We next evaluated the coherence between gamma-band power and pupil diameter during different arousal states (using GLME models) and at two different frequencies. The specific frequencies (0.02, 0.35 Hz) were chosen for statistical comparison as they were the approximate peaks in pupil–gamma power coherence during the *Asleep* and *Alert* behavioral states. Using the Bonferroni correction for multiple comparisons (3 at 0.02 Hz, 15 at 0.35 Hz) put the adjusted significance thresholds (α) at 0.017 and 0.003, respectively. The pupil–gamma power coherence during *Alert* periods at 0.02 Hz was 0.34 ± 0.18 (Fig. 3*d*,*e*, Table 3), and was significantly elevated during periods of *Asleep* at 0.68 ± 0.09 ($p = 2.4 \times 10^{-18}$) and during *All* data at 0.48 ± 0.19 ($p = 2.9 \times 10^{-5}$). Pupil–gamma power coherence at 0.35 Hz (Fig. 3*d*,*f*, Table 4) during periods of awake *Rest* and *Alert* were similar at 0.2 ± 0.1 and 0.2 ± 0.09, respectively ($p = 0.58$), similar to what is seen between the pupil diameter and cortical neuron membrane potential (McGinley et al., 2015). The coherence of all other arousal states at 0.35 Hz was significantly lower than those of the nonsleep states (*NREM*, 0.09 ± 0.06, $p = 2.9 \times 10^{-13}$; *REM*, 0.14 ± 0.08, $p = 3.7 \times 10^{-5}$; *Asleep*, 0.11 ± 0.07, $p = 9.8 \times 10^{-9}$; *All*, 0.11 ± 0.08, $p = 5.3 \times 10^{-9}$).

We then looked at how the relationship between pupil diameter and cortical blood volume changed with arousal state. During the 'Awake' state in the absence of stimulation, fluctuations in pupil diameter and hemodynamic signals were small. When the animals were in 'REM' and 'NREM' sleep, the pupil constricted, whereas blood volume increased substantially (Fig. 3*g*). We then looked at the cross-correlation between Δ[HbT] and pupil diameter to determine their temporal relationship. We saw the extrema of the cross-correlation during awake *Rest* was −0.37 ± 0.25 at a lag of 1.13 s, such that pupil diameter changes occurred on average 1.13 s before hemodynamic oscillations, and pupil diameter was negatively correlated with blood volume (Fig. 3*h*). *NREM* was more strongly anticorrelated than

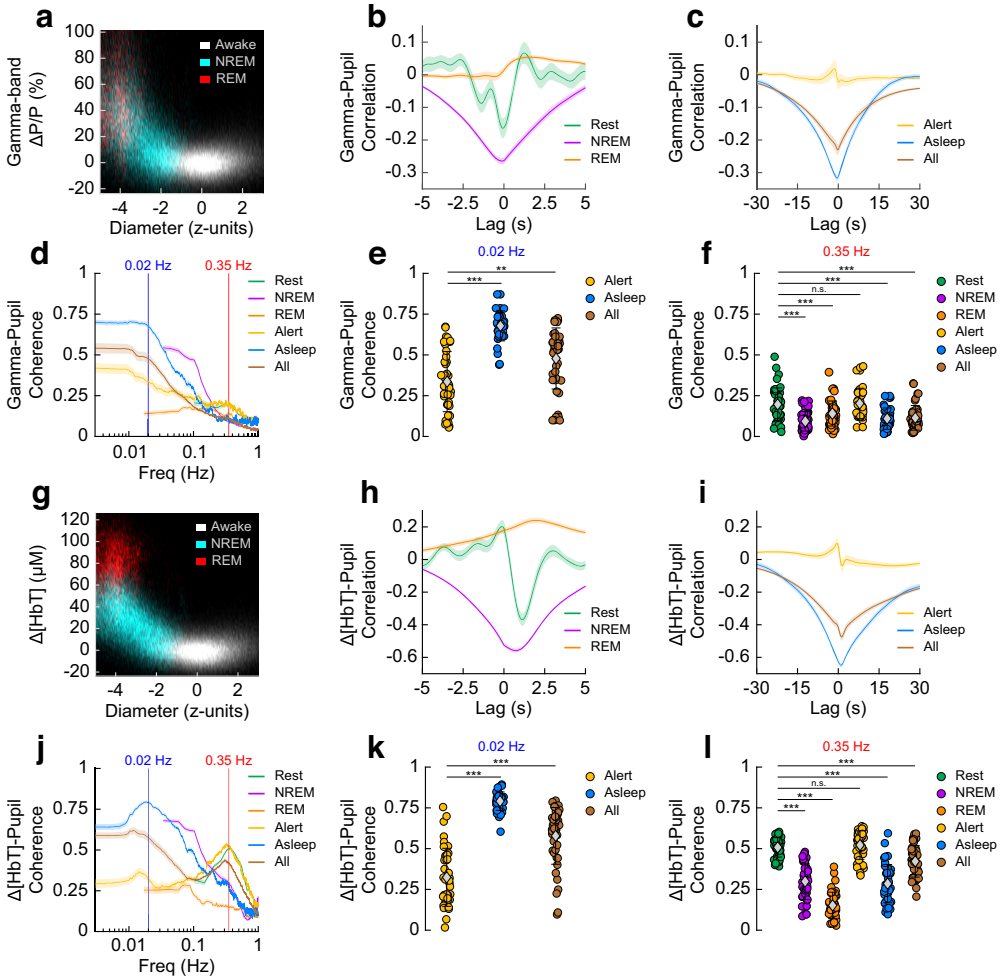

Figure 3. Pupil diameter shows an arousal-state-dependent negative correlation with blood volume and gamma-band power. ***a–f***, Relationship between gamma-band power and pupil diameter. Two-dimensional histogram showing the relationship between pupil diameter and gamma-band power during the three arousal state classes (***a***). Cross-correlation between gamma-band power and pupil diameter for short duration arousal states (***b***). Cross-correlation for longer duration arousal states (***c***). Coherence between gamma-band power and pupil diameter (***d***). Coherence at 0.02 Hz between gamma-band power and pupil diameter (***e***). Coherence at 0.35 Hz (***f***). ***g–l***, Relationship between Δ[HbT] and pupil diameter. Two-dimensional histogram showing the relationship between pupil diameter and blood volume during the three arousal state classes (***g***). Cross-correlation between pupil diameter and blood volume for short duration arousal states (***h***). Cross-correlation for long duration arousal states (***i***). Coherence between pupil diameter and blood volume (***j***). Coherence at 0.02 Hz (***k***). Coherence at 0.35 Hz (***l***). Shading (***b***, ***c***, ***h***, ***i***) indicates SEM. Error bars (***d***, ***e***, ***f***, ***j***, ***k***, ***l***) indicate SD. Statistics comparisons shown are between *Rest*/*Alert* and other arousal states using a GLME mode with Bonferroni correction for multiple comparisons (3 in ***e***, ***k***, $*\alpha < 0.017$, $**\alpha < 0.003$, $***\alpha < 0.0003$; or 15 in ***f***, ***l***, $*\alpha < 0.003$, $**\alpha < 0.00{,}067$, $***\alpha < 0.000067$, n.s.). Tables 3, 4, 5, and 6 contain additional statistical comparisons between each arousal state in (***e***, ***f***, ***k***, ***l***).

Table 3. Statistical comparisons of pupil–gamma power coherence at 0.02 Hz

	Alert	Asleep	All
Alert		***2.4 × 10−18	**2.9 × 10−4
Asleep	***2.4 × 10−18		***5.0 × 10−9
All	**2.9 × 10−4	***5.0 × 10−9	

Bonferroni-corrected significance levels (3), $*\alpha < 0.017$, $**\alpha < 0.003$, $***\alpha < 0.0003$.

Rest at −0.56 ± 0.08 at 0.73 s. *REM* had a maximum positive correlation of 0.24 ± 0.11 at 1.97 s. The peak of the Δ[HbT] and pupil diameter correlation in the *Alert* condition was 0.1 ± 0.21 at −0.43 s; this negative lag is likely because of sustained bouts of whisking (Fig. 3*i*). *Asleep* and *All* were anticorrelated at −0.65 ± 0.08 at a lag time of 1.0 s, and −0.48 ± 0.15 at a lag of 1.23 s, respectively. Generally, pupil dilations preceded vasoconstriction by about a second.

For nearly all cases, the coherence between hemodynamic signals and pupil diameter was substantially higher at lower frequencies. We evaluated the pupil–Δ[HbT] coherence during different arousal states at 0.02 Hz (Fig. 3*j*,*k*, Table 5) and 0.35 Hz (Fig. 3*j*,*l*, Table 6). As with the comparisons between pupil diameter and gamma-band power, these specific frequencies were chosen for statistical comparison (GLME) as they were the approximate peaks in pupil–Δ[HbT] coherence during *Asleep* behaviors and *Alert* behaviors, respectively. A Bonferroni correction for multiple comparisons (3 comparisons at 0.02 Hz, 15 at 0.35 Hz) put the adjusted significance threshold (α) at 0.017 and 0.003, respectively. At 0.02 Hz, coherence between total hemoglobin and pupil diameter during the *Alert* state was 0.32 ± 0.18 (N = 20 mice). As we can only evaluate the 0.02 Hz component of the spectrum in the longer 15-min-duration epochs, statistical comparisons were only done for longer duration behavioral conditions. Pupil–Δ[HbT] coherence during *Asleep* periods was 0.79 ± 0.06 ($p = 2.0 \times 10^{-29}$) and *All* periods was 0.58 ± 0.17 ($p = 9.3 \times 10^{-14}$). At 0.35 Hz, *Rest* had a pupil–Δ[HbT] coherence of 0.51 ± 0.06 (N = 22 mice). The pupil–Δ[HbT] coherence during rest was not significantly different from that during the *Alert* behavior, being 0.52 ± 0.09 (p = 0.33). However, the coherence at 0.35 Hz was significantly lower during all sleep associated periods (*NREM*, 0.3 ± 0.11, $p = 7.0 \times 10^{-33}$; *REM*, 0.15 ± 0.08, $p = 9.8 \times 10^{-66}$;

Table 4. Statistical comparisons of pupil–gamma power coherence at 0.35 Hz

	Rest	NREM	REM	Alert	Asleep	All
Rest		***2.9 × 10–13	***3.7 × 10–5	0.58	***9.8 × 10–9	***5.3 × 10–9
NREM	***2.9 × 10–13		**0.0005	***3.2 × 10–14	0.12	0.10
REM	***3.7 × 10–5	**0.0005		***5.6 × 10–6	0.07	0.07
Alert	0.58	***3.2 × 10–14	***5.6 × 10–6		***1.2 × 10–9	***6.2 × 10–10
Asleep	***9.8 × 10–9	0.12	0.07	***1.2 × 10–9		0.96
All	***5.3 × 10–9	0.10	0.07	***6.2 × 10–10	0.96	

Bonferroni-corrected significance levels (15), *$\alpha < 0.003$, **$\alpha < 0.00{,}067$, ***$\alpha < 0.000067$.

Table 5. Statistical comparisons of pupil-Δ[HbT] coherence at 0.02 Hz

	Alert	Asleep	All
Alert		***2.0 × 10–29	***9.3 × 10–14
Asleep	***2.0 × 10–29		***1.3 × 10–10
All	***9.3 × 10–14	***1.3 × 10–10	

Bonferroni-corrected significance levels (3), *$\alpha < 0.017$, **$\alpha < 0.003$, ***$\alpha < 0.0003$.

Asleep, 0.29 ± 0.12, $p = 2.5 \times 10^{-33}$; *All*, 0.42 ± 0.1, $p = 3.4 \times 10^{-8}$).

Low-frequency fluctuations in blood volume are highly correlated with the pupil diameter, suggesting that the same processes that modulate arousal on these timescales also cause constriction in the cerebral vasculature. There was a strong negative correlation between pupil diameter and blood volume as well as between pupil diameter and gamma-band power during periods of *Rest* and *Asleep*, with these correlations turning positive during periods of alertness and active whisking. This is in general consistent with an anticorrelation between arousal level and blood volume (Cardoso et al., 2019) in the absence of stimulation or active whisking behavior.

Blinking is associated with increases in arousal

We next explored the relationship between blinking and arousal level. The mean interblink interval was 117.4 ± 33.6 s (Fig. 4*a*,*b*; $N = 22$ mice). We then quantified the probability of a blink being elicited by sensory stimulation of the whiskers. Except for one animal, our mice did not frequently blink after a whisker stimulation, with the mean probability of blinking within 5 s poststimulus being only 5.4 ± 5.1% (Fig. 4*c*; $N = 21$ mice, excluded mouse at 25.6%). For blinks that did occur following stimulation, blinks typically occurred within a half second (~37%), and the probability decreased thereafter. Blinks primarily occurred during the 'Awake' state (>70%), but when they did occur during periods of 'REM' or 'NREM' sleep the animal either quickly returned to sleep after a brief awakening or did not wake up at all (Fig. 4*d*). Blinking events also occurred during periods of maintained REM sleep with no awakening. The likelihood of volitional whisking occurring simultaneously with blinking behavior was high (Fig. 4*e*), with volitional whisking occurring during 40% of 'Awake' blink events. Whisking was less frequent during blinks that occurred either during or immediately following periods classified as 'Asleep' (with the majority being in 'NREM').

As blinks commonly occurred in clusters, for all blink-related analysis we only looked at the first blink occurring in a string of blink events that occurred within <1 s of each other. All blinks that occurred within ±5 s of whisker stimulation were also excluded to prevent the stimulus from interfering with the blink-triggered comparison. To help separate the effect of the blink from the effects of volitional whisking behavior coinciding with it, we split the dataset into low-whisk blinks (LWBs) and high-whisk blinks (HWBs), further split by whether they occurred when the mouse was 'Awake' or 'Asleep' ('REM' and 'NREM' combined). LWBs were defined as events where the mouse was whisking for <1/3 of a second in the 2 s surrounding each blink, whereas HWBs were defined as whisking for >1 s within ±2 s of the blink. We evaluated blink-triggered averages for changes in diameter (*z*-units), Δ[HbT], EMG power, cortical LFP, and hippocampal LFP across all blinks from all mice that met the criteria. During the 'Awake' state, LWBs caused an increase of ~0.7 *z*-units in pupil diameter compared with resting baseline, whereas HWBs caused an increase in excess of 3 *z*-units (Fig. 4*f*). Δ[HbT] during LWBs increased ~4 μM from the period before the blink, whereas HWB increased ~10 μM, probably because of the increased whisking in the time preceding the blink (Fig. 4*g*). EMG power increases ~0.6 orders of magnitude during LWBs compared with 1.2 orders of magnitude during HWBs, with power increases starting ~0.5 s before the blink occurs. There were negligible increases in gamma-band power in both the somatosensory cortex (Fig. 4*i*) and the hippocampus (Fig. 4*k*) during LWBs, with the ~20% increases in power seen during high whisking likely being because of the whisking (Winder et al., 2017) and not the blink (Fig. 4*j*,*l*).

Blink-associated neural and vascular changes were similar during blinks that occurred during periods of 'Asleep,' with the caveat that the baseline pupil diameter was lower. Pupil diameter during both high- and low-whisk asleep blinks was small before the blink (less than −3 *z*-units), with the diameter slowly increasing preceding the blink as the animal began to wake up. For periods of low whisking, the pupil remained constricted as the animals presumably fell back asleep or remained asleep (Fig. 4*m*). Changes in hemodynamics followed a similar trend, with there being a reduction in total hemoglobin in the time preceding the blink as the animals are waking up (Fig. 4*n*). EMG power changes were similar to the 'Awake' blink but with a lower baseline power (Fig. 4*o*). We noted no appreciable differences among the blink-associated power spectra during blinks that occurred around sleeping periods (Fig. 4*p–s*), however the drop in cortical delta power around the blink is evident as the animals wake up from sleep (which was predominantly NREM). Altogether, blinking was associated with increases in arousal, but to varying degrees marked by differing amounts of accompanying whisking. When blinks occurred during the 'Awake' state, there was only a small increase in blood volume if there was minimal whisking. However, when blinks occurred during the 'Asleep' state, large decreases in blood volume followed regardless of whisking amount.

Awake blinking causes a resetting of neural and vascular dynamics

We next asked how blinking is correlated with the neural and vascular synchrony between bilateral regions of somatosensory cortex. Processing of new or startling information is

Table 6. Statistical comparisons of pupil–Δ[HbT] coherence at 0.35 Hz

	Rest	NREM	REM	Alert	Asleep	All
Rest		***7.0 × 10−33	***9.8 × 10−66	0.33	***2.5 × 10−33	***3.4 × 10−8
NREM	***7.0 × 10−33		***2.6 × 10−19	***6.9 × 10−35	0.59	***1.4 × 10−14
REM	***9.8 × 10−66	***2.6 × 10−19		***1.0 × 10−66	***7.7 × 10−17	***7.1 × 10−47
Alert	0.33	***6.9 × 10−35	***1.0 × 10−66		***2.6 × 10−35	***3.9 × 10−10
Asleep	***2.5 × 10−33	0.59	***7.7 × 10−17	***2.6 × 10−35		***1.9 × 10−15
All	***3.4 × 10−8	***1.4 × 10−14	***7.1 × 10−47	***3.9 × 10−10	***1.9 × 10−15	

Bonferroni-corrected significance levels (15), *$\alpha < 0.003$, **$\alpha < 0.00{,}067$, ***$\alpha < 0.000067$.

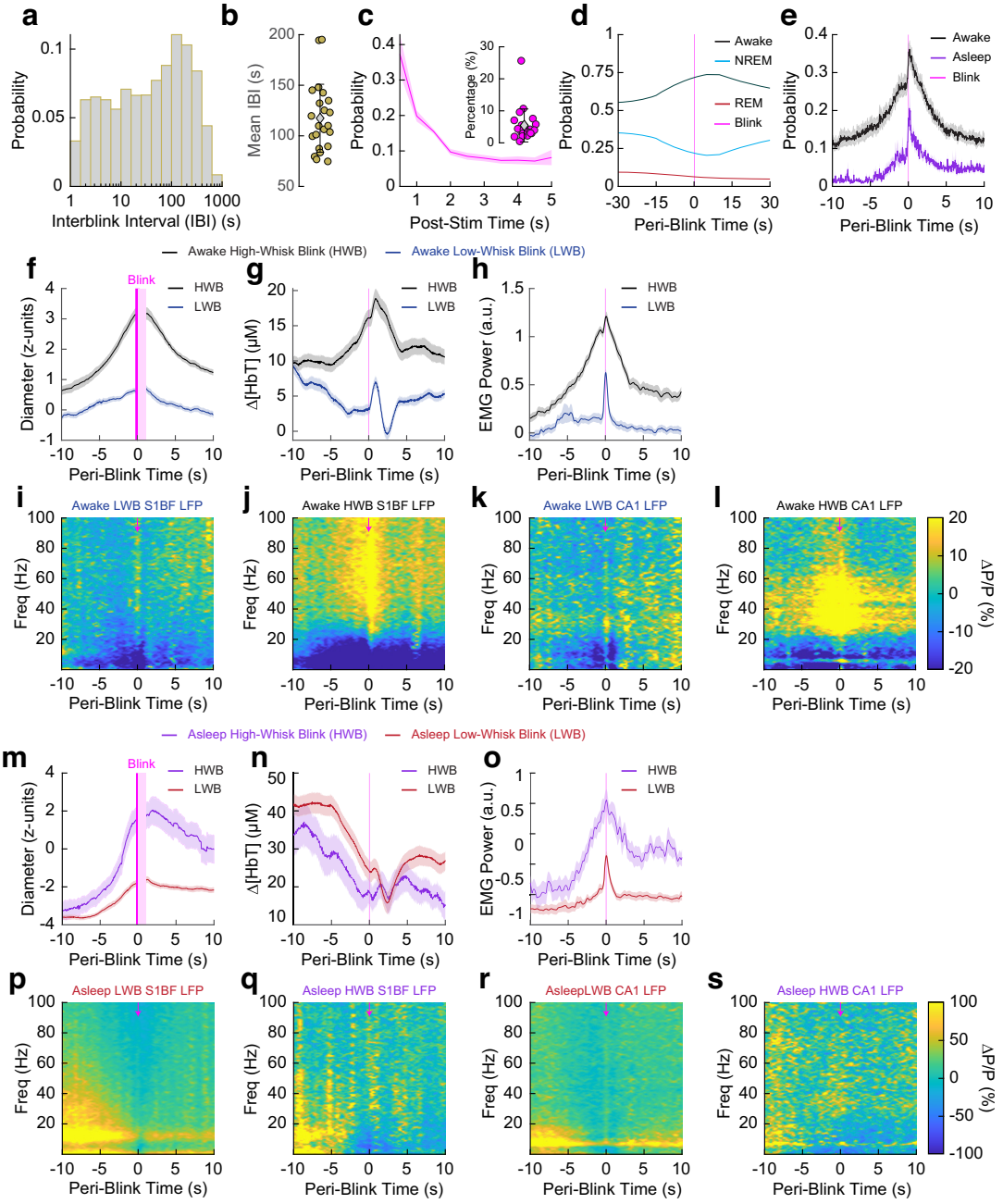

Figure 4. Blink-triggered neural and blood volume responses show arousal-state-dependent changes. ***a***, Histogram of interblink interval for all blinks. ***b***, Mean interblink interval from each animal. ***c***, Histogram of poststimulus (Post-stim) probability of a blink for whisker stimulations that elicited a blink. Inset, Mean probability from each animal of blinking after a whisker stimulus. ***d***, Periblink arousal states. ***e***, Periblink probability of whisking during 'Awake' or 'Asleep' periods. ***f–l***, Blink-triggered averages for blinks that occurred during an 'Awake' period, separated into either HWBs or LWBs. Periods where the pupil is partially obscured by the eyelid have been censored (pink). Pupil diameter during 'Awake' blinks (***f***). Hemodynamics during 'Awake' blinks (***g***). Electromyography during 'Awake' blinks (***h***). Cortical LFP during 'Awake' LWBs (***i***). Cortical LFP during 'Awake' HWBs (***j***). Hippocampal LFP during 'Awake' LWBs (***k***). Hippocampal LFP during 'Awake' HWBs (***l***). ***m–s***, Blink-triggered averages for blinks that occurred during an 'Asleep' period, separated into either HWB or LWB events. Pupil diameter during 'Asleep' blinks (***m***). Hemodynamics during 'Asleep' blinks (***n***). Electromyography during 'Asleep' blinks (***o***). Cortical LFP during 'Asleep' blinks with low amounts of whisking (***p***). Cortical LFP during 'Asleep' blinks with high amounts of whisking (***q***). Hippocampal LFP during 'Asleep' LWBs (***r***). Hippocampal LFP during 'Asleep' HWBs (***s***). Scatter plot error bars (***b***, ***c***, inset) indicate SD. Shading (***c*** main, ***e–h***, ***m–o***) indicates SEM.

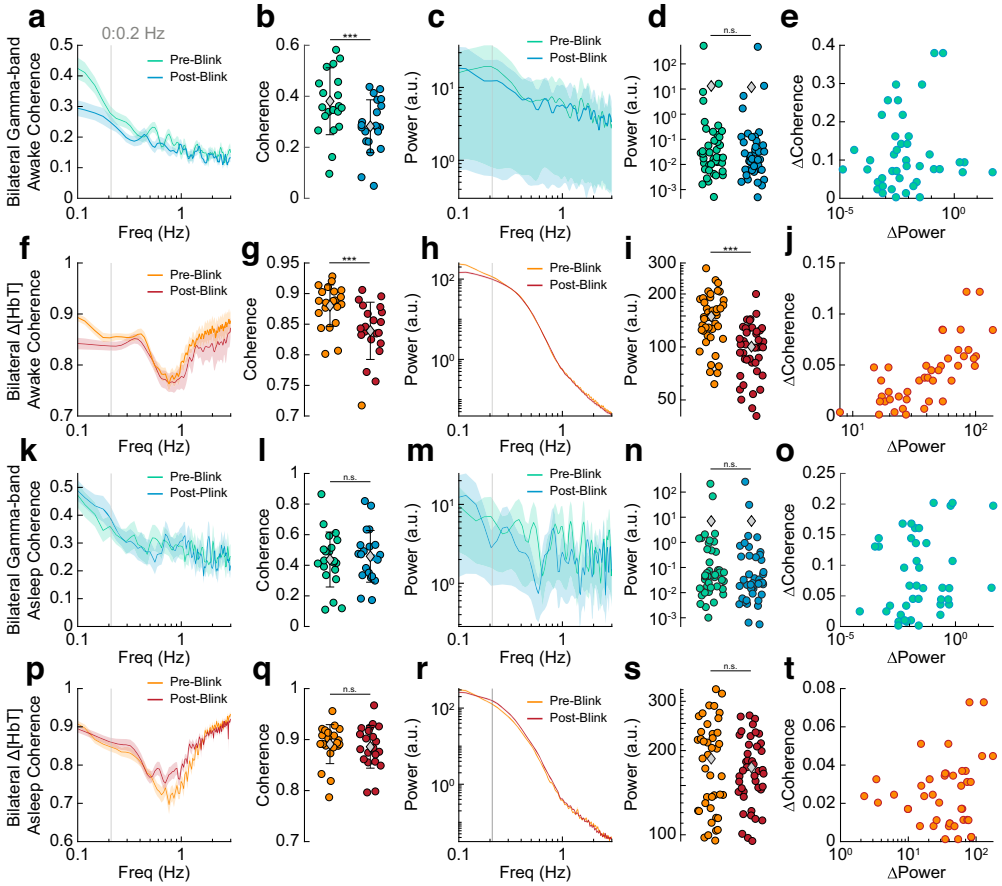

Figure 5. Effects of blinking on neural and bilateral hemodynamic signals. ***a***, Coherence between left and right gamma-band power before and after an awake blink. ***b***, Mean coherence from 0 to 0.2 Hz before and after an awake blink. ***c***, Power spectrum of gamma-band power envelope before and after an awake blink. ***d***, Mean power between 0 and 0.2 Hz before and after an awake blink. ***e***, Change in preblink versus postblink gamma-band power versus change in preblink versus postblink gamma-band coherence for awake blinks. ***f***, Coherence between left and right Δ[HbT] before and after an awake blink. ***g***, Mean coherence between left and right Δ[HbT] signals between 0 and 0.2 Hz before and after an awake blink. ***h***, Δ[HbT] power before and after an awake blink. ***i***, Mean power between 0 and 0.2 Hz before and after an awake blink. ***j***, Change in preblink versus postblink power versus change in preblink versus postblink coherence for awake blinks. ***k***, Coherence between bilateral gamma-band signals before and after an asleep blink. ***l***, Mean coherence between bilateral gamma-band signals between 0 and 0.2 Hz before and after an asleep blink. ***m***, Power spectrum of the gamma-band power envelope before and after an asleep blink. ***n***, Mean power in the gamma-band envelope between 0 and 0.2 Hz before and after an asleep blink. ***o***, Change in preblink versus postblink power versus change in preblink versus postblink coherence for asleep blinks. ***p–t***, Δ[HbT] before and after an asleep blink. Coherence between bilateral hemodynamic signals before and after a blink during sleep (***p***). Mean coherence between 0 and 0.2 Hz before and after an asleep blink (***q***). Δ[HbT] power before and after an asleep blink (***r***). Mean power between 0 and 0.2 Hz before and after an asleep blink (***s***). Change in preblink versus postblink power versus change in preblink versus postblink coherence for asleep blinks (***t***). Error bars (***b***, ***d***, ***g***, ***i***, ***l***, ***n***, ***q***, ***s***) indicate SD. Shading (***a***, ***c***, ***f***, ***h***, ***k***, ***m***, ***p***, ***r***) indicates SEM. Paired *t* test, $*\alpha < 0.05$, $**\alpha < 0.01$, $***\alpha < 0.001$, n.s.

accompanied by blinking, suggesting it is associated with some sort of mental resetting (Siegle et al., 2008). As before, we separated blinks by arousal state ('Awake,' 'Asleep') and looked at the changes in power and coherence during periods preceding (−15 to −5 s) and following (5 to 15 s) each blink. We excluded the time ±5 s adjacent to each blink to capture the pre-effects and posteffects of the blink on synchrony and not the blink itself, as the blink elicits brief changes in neural activity and blood volume, and this response will drive coherence across all frequencies temporally close to the blink that reflect the evoked activity, not necessarily a state change in the brain. For both bilateral cortical gamma-band power signals and bilateral changes in Δ[HbT], we evaluated the power/coherence changes from 0 to 0.2 Hz as this corresponded to the frequency domain of the largest difference between the preblink and postblink intervals. One animal was excluded from the analysis in Figure 4 because of being an outlier in its blink rate (N = 21). Coherence between bilateral gamma-band power signals during the 'Awake' state dropped following a blink from 0.38 ± 0.13 preblink to 0.28 ± 0.10 postblink (p = 0.001, paired t test; Fig. 5*a*,*b*). Power in these signals (Fig. 5*c*) did not change in the period following a blink (13.2 ± 81.0 a.u. preblink vs 11.9 ± 73.7 a.u. postblink; p = 0.25, paired t test; Fig. 5*d*). There was no clear relationship between changes in gamma-band power preblink versus postblink versus changes in bilateral gamma-band coherence preblink versus postblink (Fig. 5*e*). 'Awake' bilateral Δ[HbT] coherence was 0.88 ± 0.03 preblink, dropping to 0.84 ± 0.05 postblink ($p = 6.4 \times 10^{-6}$; Fig. 5*f*,*g*). Unlike the gamma-band power, there was a significant drop in cortical hemodynamic power following a blink (149.1 ± 49.1 a.u. preblink vs 100.4 ± 33.3 a.u. postblink; $p = 8.2 \times 10^{-13}$, paired t test; Fig. 5*h*,*i*), and these appear to be related (Fig. 5*j*).

For blinks that occurred during the 'Asleep' state, neither the gamma-band power nor total hemoglobin showed any significant changes between preblink and postblink power or coherence. The mean coherence from 0 to 0.2 Hz between bilateral gamma-band signals during 'Asleep' blinks was 0.44 ± 0.18 preblink versus 0.46 ± 0.17 postblink (p = 0.38, paired t test; Fig. 5*k*, *l*) with power changes of 7.0 ± 34.4 preblink versus 7.1 ± 39.9 postblink (p = 0.98, paired t test; Fig. 5*m*,*n*), with no relationship

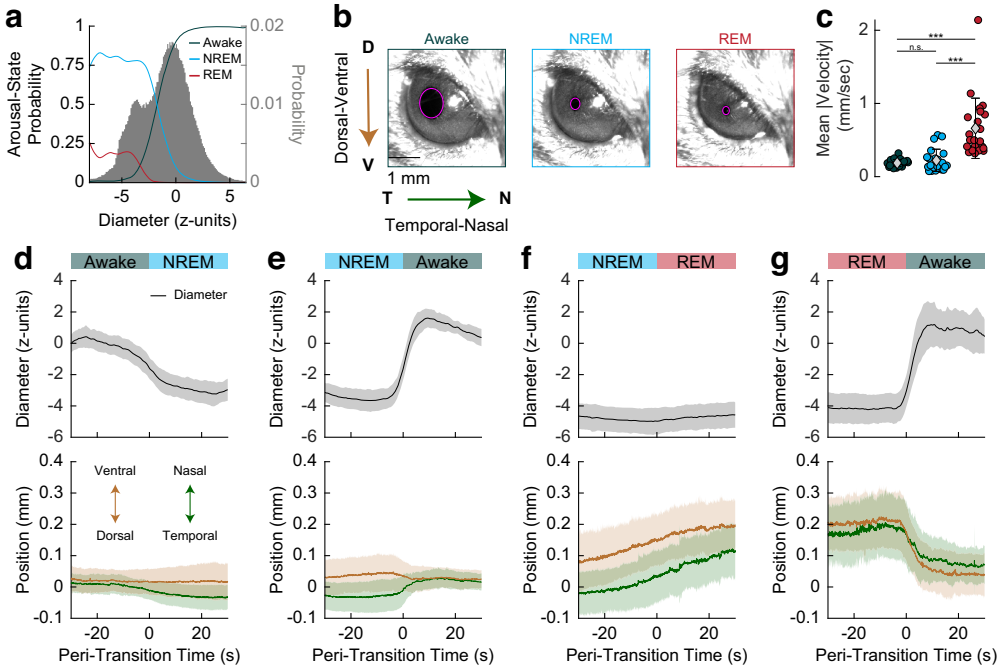

Figure 6. Pupil size, position, and motion change with arousal state. ***a***, Probability of arousal state classification as a function of pupil diameter. ***b***, Diagram demonstrating the drift of the pupil as the animal falls to sleep. The position of the centroid is measured relative to the resting location. ***c***, Mean absolute velocity of the eye in each arousal state. ***d–g***, Pupil diameter (top) and pupil position (bottom) as the animal transitions from one arousal state to another. During REM sleep, the eye rotated toward the nose (nasally) and ventrally. Error bars and shading indicate SD. Bonferroni-corrected (3) paired *t* test, *$\alpha < 0.017$, **$\alpha < 0.003$, ***$\alpha < 0.0003$, n.s.

between power and coherence changes (Fig. 5*o*). Bilateral hemodynamic coherence during 'Asleep' blinks was 0.89 ± 0.04 preblink versus 0.89 ± 0.04 postblink ($p = 0.45$, paired *t* test; Fig. 5*p*,*q*) at a power of 187.1 ± 67.1 preblink versus 174.1 ± 47.3 postblink ($p = 0.17$, paired *t* test; Fig. 5*r*,*s*), with no relationship between power and coherence changes (Fig. 5*t*). These results indicate that blinking during the 'Awake' state was correlated with a resetting of neural and vascular signals, but this did not happen with blinks during 'Asleep.'

Pupil size, position, and motion change with arousal state

When looking at the probability of being in a given arousal state as a function of pupil diameter (Fig. 6*a*), it is apparent that the probability of wakefulness decreases dramatically as the pupil decreases in size with the 50% probability (that is, equal probability of being awake or asleep) being around −2 *z*-units from the resting baseline. However, the pupil size in our dataset was similar across *REM* and *NREM* sleep states. We next asked how other eye metrics could help differentiate further between REM and NREM sleep, as previous work has found systematic changes in eye position of rodents during REM (Sánchez-López and Escudero, 2011). When the animals fall asleep, the pupil begins to drift as the muscles around the eye relax. There are also rapid-eye-movements characteristically seen during REM sleep. We tracked the centroid of the pupil (Fig. 6*b*) and changes in its position measured relative to the resting location. When looking at the eye velocity in each arousal state (Fig. 6*c*), we see that the pupil moves significantly more during 'REM' sleep (0.66 ± 0.41 mm/s) than in either the 'Awake' (0.19 ± 0.05 mm/s, $p = 1.8 \times 10^{-5}$) or 'NREM' states (0.22 ± 0.15 mm/s, $p = 1.5 \times 10^{-5}$). Despite a large change in diameter, there was minimal change in pupil centroid location during transitions between the 'Awake' and 'NREM' states (Fig. 6*d*,*e*). However, the centroid of the pupil moves between 0.1 and 0.2 mm in the nasal and ventral directions when the animal transitions into the 'REM' state (Fig. 6*f*) and quickly returns to the baseline location on awakening (Fig. 6*g*).

Eye metrics are an accurate predictor of arousal state

Finally, we explored using eye metrics (pupil diameter and position) alone as a predictor of arousal state, comparing their predictive power to that of more conventional sleep scoring using physiological parameters (cortical delta power, hippocampal theta power, EMG). As pupil diameter is commonly measured in behaving mouse paradigms (McGinley et al., 2015; Vinck et al., 2015; Pisauro et al., 2016; Musall et al., 2019; Stringer et al., 2019; Aguillon-Rodriguez et al., 2021), arousal scoring using pupil diameter and eye movement could be very useful for detecting bouts of sleep when other more invasive assays are not available. Previous work has shown that the sleep/wake state of head-fixed mice can be determined accurately on the timescale of hundreds of seconds using pupil diameter (Yüzgeç et al., 2018), but here we asked whether it can be done on a timescale of seconds.

Pupil diameter alone could be used to differentiate the 'Awake' arousal state from the 'REM' and 'NREM' states (with a threshold at approximately −2 *z*-units, Fig. 6*a*). However, there was much less difference in pupil diameter between the two sleep states. Therefore, we used the position and motion of the centroid of the pupil in our model classification to achieve a separation between 'REM' and 'NREM.' We compared the manual scores of an exemplar 15 min imaging session to those produced by three different bootstrapped random forest classification models (Fig. 7*a*) following model training using a 70:30 training/testing split. The first model used only eye metrics, such as the diameter of the pupil (mm, *z*), position, and average velocity (Eye Model; see above, Materials and Methods). We used the same example data shown in Figure 1*f* to show how these three metrics can be used to identify arousal state (Fig. 7*b–d*). The

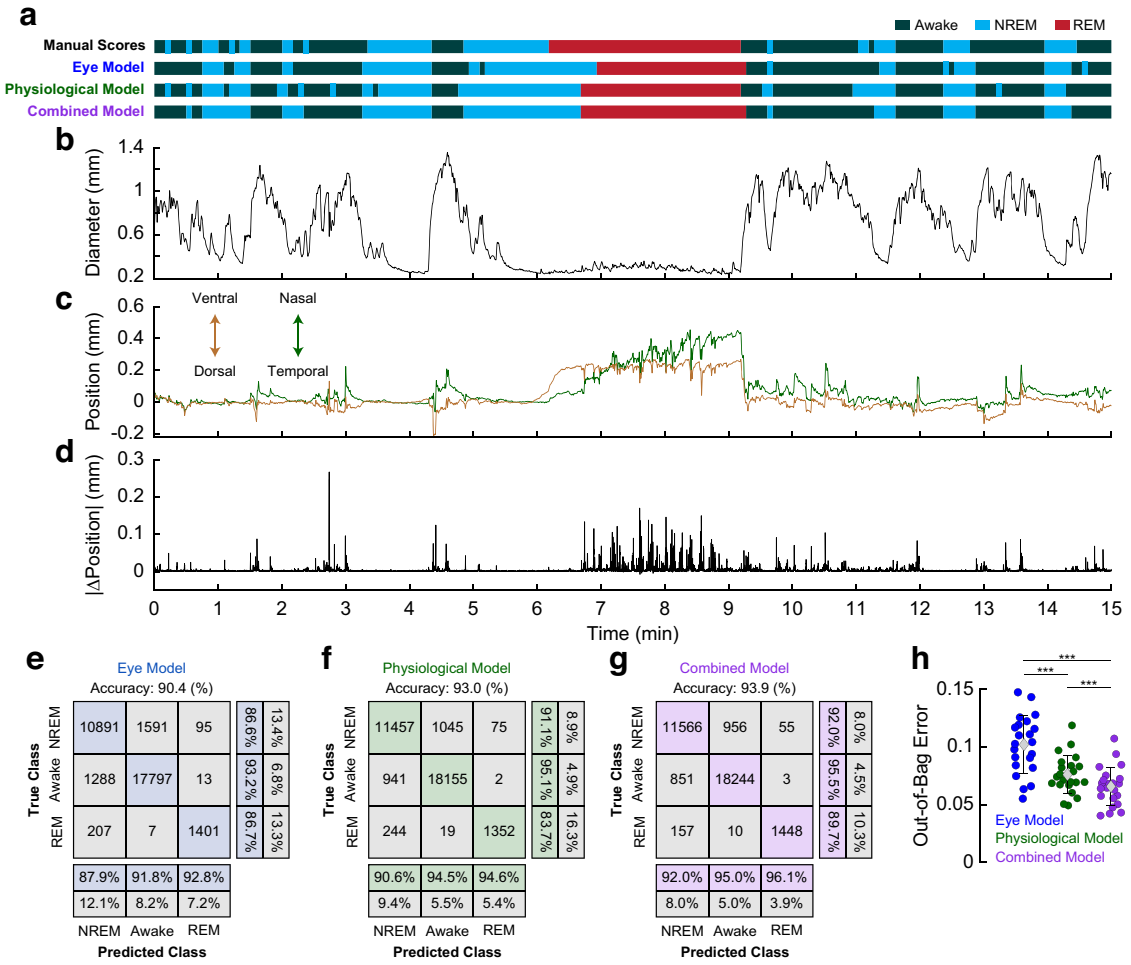

Figure 7. Eye metrics alone are an accurate predictor of arousal state. ***a***, Arousal state predictions from three arousal state classification models (Eye, Physiologic, Combined) and manual scores for sample data. Data are the same as presented in Figure 1. ***b***, Example trace of pupil diameter over time with respect to arousal state. For clarity, blinks are not shown. ***c***, Position of the pupil changes when the animal goes into REM sleep, moving nasally and ventrally. ***d***, Absolute change in the frame-by-frame position of the pupil indicates a high degree of movement during 'REM' sleep. ***e***, Confusion matrix of a bagged random forest (70:30% training/testing) using only eye metrics such as pupil diameter, position, and motion (Eye Model). ***f***, Confusion matrix of a bagged random forest (70:30% training/testing) using measurements of cortical and hippocampal LFP, electromyography, heart rate, and whisker motion (Physiologic Model). ***g***, Confusion matrix of a model using both the eye and physiological data (Combined Model) for arousal scoring. ***h***, Out-of-bag error estimation during model training for each model. Error bars (***h***) indicate SD. Bonferroni-corrected (3) paired *t* test, $^{*}\alpha < 0.017$, $^{**}\alpha < 0.003$, $^{***}\alpha < 0.0003$, n.s.

pupil decreases in size during 'REM' and 'NREM' sleep compared with the awake state, but it is the changes in pupil position that separate 'REM' from 'NREM' sleep. The second model was identical to that used in Turner et al. (2020) and used seven physiological parameters (i.e., Physiological Model; see above, Materials and Methods). The third model was a combination of the two (Combined Model), using both eye metrics and the physiological measurements. With respect to identifying sleep, the Eye Model ($N = 22$ mice) had a total cumulative accuracy of 90.4% across all testing data (Fig. 7*e*) with comparable Type I and Type II classification errors. The Physiological Model (cumulative accuracy of 93.0%; Fig. 7*f*) and combined model (cumulative accuracy of 93.9%; Fig. 7*g*) performed better than the eye model, having access to the "gold-standard" of electrophysiology and electromyography information classically used for detecting sleep. The out-of-bag error during model training was higher for the Eye Model (0.10 ± 0.02) than the Physiological Model (0.08 ± 0.02, $p = 7.0 \times 10^{-6}$), as well for as the Combined Model (0.07 ± 0.02, $p = 5.2 \times 10^{-10}$; Fig. 7*h*). However, the eye metrics did significantly improve the Combined Model over the original Physiological Model ($p = 1.0 \times 10^{-6}$). Our findings indicate that monitoring the eye, including pupil diameter and its changes in position, can be used as a noninvasive method to determine whether head-fixed mice are sleeping on a timescale of seconds.

Discussion

In this study, we explored the relationship between pupil diameter and blinking with ongoing neural activity and hemodynamic signals in the somatosensory cortex of mice during different arousal and behavioral states. Pupil diameter was consistently smaller during sleep states and larger during the awake state, allowing the pupil to be used as a predictor of arousal state (Yüzgeç et al., 2018). As a practical matter, a threshold of ~2 *z*-units below the resting pupil diameter can function as an indicator of sleep. Blinking was correlated with changes in arousal levels, as well as with neural and vascular dynamics. Mice were more likely to be in the awake state after blinking than before, and bilateral synchronization in the gamma-band envelope and accompanying hemodynamics both decreased after blinks when the mouse was awake. The difference in neural responses to blinks in the awake versus

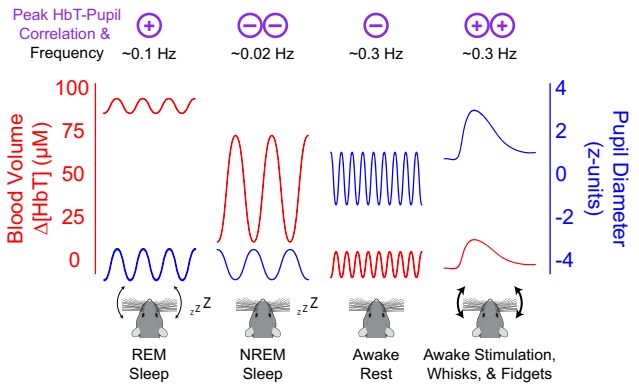

Figure 8. Pupil diameter is anticorrelated with cortical hemodynamics during Rest and NREM sleep. Summary schematic demonstrating the observed correlation between pupil diameter and cortical hemodynamics during each arousal state. Correlations between pupil diameter and blood volume are positive during REM sleep and when the mouse is alert, moving, or stimulated. Correlations between pupil diameter and blood volume are negative during rest and NREM sleep. Although the oscillation amplitude and baseline offset of the pupil diameter/blood volume reflect what is observed in our data, for clarity the temporal frequencies of oscillations are not to scale.

asleep conditions could be because of differences in sensory processing in these respective states.

Because our mice slept frequently, when averaged over the entire dataset, the pupil diameter was strongly anticorrelated with both gamma-band power and blood volume because of the large vasodilation occurring during NREM sleep (Turner et al., 2020). When restricted to just data in the awake state, whose neural and hemodynamic signals are dominated by body movements and fidgeting behavior (Huo et al., 2014; Winder et al., 2017; Tran et al., 2018; Drew et al., 2019; Musall et al., 2019; Stringer et al., 2019; Drew et al., 2020; Salkoff et al., 2020), the pupil diameter was positively correlated with gamma-band power and blood volume (Fig. 8). The coherence between blood volume and pupil diameter was stronger at lower frequencies and was highest (>0.75) at 0.02 Hz (corresponding to ~50 s period) in the sleeping mouse. Interestingly, activity in the LC and the concentration of noradrenaline during NREM sleep fluctuates on a similar timescale (Osorio-Forero et al., 2021; Kjaerby et al., 2022). As noradrenaline is vasoconstrictory (Raichle et al., 1975; Goadsby et al., 1985; Bekar et al., 2012), the fluctuations in noradrenaline during NREM may contribute to the oscillations in blood volume (Fultz et al., 2019; Turner et al., 2020), which simulations and experiments have suggested are important for clearing waste from the brain (Xie et al., 2013; Kedarasetti et al., 2020a,b; van Veluw et al., 2020; Kedarasetti et al.,2022). The fact that there is vasodilation in somatosensory cortex during periods of body motion and arousal when noradrenaline levels are highest can be accounted for by the action of local vasodilatory signals from neurons during behavior (Winder et al., 2017; Zhang et al., 2019; Echagarruga et al., 2020). Although our LFP measurements were conducted in the somatosensory cortex, we would expect similar dynamics in other sensory areas of the cortex, such as visual areas, which are innervated by the same LC neurons (Kim et al., 2016). The vascular dynamics may differ in the frontal cortex and other areas, which receive input from a different subset of LC neurons (Kim et al., 2016).

Our findings that the pupil diameter was strongly anticorrelated with blood volume should be taken in the context of the literature relating arousal and pupil diameter to LC activity and the vasoconstrictory impact of noradrenergic inputs of LC on the cerebral vasculature. The noradrenaline levels in the brain correspond with LC neuron cell body activity (Berridge and Abercrombie, 1999; Feng et al., 2019; Poe et al., 2020). Sensory stimuli drive increases in LC neural activity, noradrenergic tone, and pupil dilation (Gilzenrat et al., 2010; Murphy et al., 2014; Schwarz and Luo, 2015; Joshi et al., 2016; Gray et al., 2021; Yang et al., 2021), although the correlations between pupil diameter and spiking of individual LC neurons is low (Megemont et al., 2022). Activation of noradrenaline-releasing neurons in the LC drive awakening from sleep (Carter et al., 2010; Hayat et al., 2020; Kjaerby et al., 2022), and this awakening from sleep is followed by profound cortical vasoconstriction (Turner et al., 2020) and brain-wide hemodynamic changes (Liu et al., 2015, 2018; Fultz et al., 2019; Zhang et al., 2022a). Electrical stimulation of the LC and subsequent increases in noradrenaline levels (Bekar et al., 2012) cause vasoconstriction (Raichle et al., 1975; Goadsby et al., 1985), but Toussay et al. (2013) observed that stimulation of the LC can increase cortical perfusion in the anesthetized rat. We saw that the blood volume–pupil diameter correlation was positive in the *Alert* state, which seems to contradict the vasoconstrictory nature of noradrenaline. The *Alert* state contains many fidgeting and whisking bouts, which can be nearly continuous body movements. Although cortical noradrenaline levels are known to rise during locomotion (Polack et al., 2013; Paukert et al., 2014) and movement (Feng et al., 2019), the activity of vasodilatory neuronal nitric oxide synthase neurons (Echagarruga et al., 2020) and vasodilatory extracellular potassium are both elevated during locomotion (Longden et al., 2017; Rasmussen et al., 2019), and these two vasodilators are likely strong enough to drive vasodilation even in the face of elevated noradrenaline. Furthermore, the magnitude of noradrenaline increases during movement are much smaller than the decreases during sleep. During sleep, microdialysis measured cortical noradrenergic levels fall >50% (Bellesi et al., 2016), although recent studies using fluorescent biosensors have shown there are large fluctuations over the timescales of minutes in noradrenaline levels in frontal areas during NREM (Kjaerby et al., 2022). The arousal-induced noradrenergic level increases during voluntary body movements and fidgeting are of a substantially smaller magnitude than the decreases seen during sleep (Feng et al., 2019), which would explain why vasodilation dominates in these behaviors. The positive correlations between pupil diameter and blood volume during REM might be because of fluctuations in cholinergic drive, which is high during REM sleep (Jing et al., 2020; Jones, 2020) and is also linked to pupil dilations (Larsen and Waters, 2018). Our observations of state-dependent correlation between blood volume and pupil diameter (Fig. 8) is consistent with noradrenergic modulation in the cortex playing a state-dependent role in neurovascular coupling in concert with local neural activity (Hamel, 2006; Kleinfeld et al., 2011).

Monitoring the pupil (Privitera et al., 2020) can provide a second-by-second insight into the sleep/wake state of mice. These periods of sleep can be an issue not only in behavioral tasks but can also be a confound in studies looking at spontaneous neural and hemodynamic activity. In human studies, sleep episodes occur frequently during resting-state imaging (Tagliazucchi and Laufs, 2014), drastically affecting functional connectivity measurements and other measures of network dynamics. In mice, bilateral neural and hemodynamic correlations are much higher during sleep (Turner et al., 2020), supporting the need for arousal-state monitoring in both animal and human studies as detecting and monitoring changes in arousal are essential for accurate interpretations of any resting-state study (Tagliazucchi and Laufs, 2014; Liu et al., 2018; Drew et al., 2020). Fortunately,

monitoring pupil diameter and eye motion can provide a simple, noninvasive way of detecting sleep and monitoring arousal state transitions in rodents.

References

Adams MD, Winder AT, Blinder P, Drew PJ (2018) The pial vasculature of the mouse develops according to a sensory-independent program. Sci Rep 8:9860.

Aguillon-Rodriguez V, et al. (2021) Standardized and reproducible measurement of decision-making in mice. Elife 10:e63711.

Amzica F, Steriade M (1998) Electrophysiological correlates of sleep delta waves. Electroencephalogr Clin Neurophysiol 107:69–83.

Bekar LK, Wei HS, Nedergaard M (2012) The locus coeruleus-norepinephrine network optimizes coupling of cerebral blood volume with oxygen demand. J Cereb Blood Flow Metab 32:2135–2145.

Bellesi M, Tononi G, Cirelli C, Serra PA (2016) Region-specific dissociation between cortical noradrenaline levels and the sleep/wake cycle. Sleep 39:143–154.

Bergel A, Deffieux T, Demené C, Tanter M, Cohen I (2018) Local hippocampal fast gamma rhythms precede brain-wide hyperemic patterns during spontaneous rodent REM sleep. Nat Commun 9:5364.

Berridge CW, Abercrombie ED (1999) Relationship between locus coeruleus discharge rates and rates of norepinephrine release within neocortex as assessed by *in vivo* microdialysis. Neuroscience 93:1263–1270.

Bokil H, Andrews P, Kulkarni JE, Mehta S, Mitra PP (2010) Chronux: a platform for analyzing neural signals. J Neurosci Methods 192:146–151.

Bradley MM, Miccoli L, Escrig MA, Lang PJ (2008) The pupil as a measure of emotional arousal and autonomic activation. Psychophysiology 45:602–607.

Breuninger T, Puller C, Haverkamp S, Euler T (2011) Chromatic bipolar cell pathways in the mouse retina. J Neurosci 31:6504–6517.

Bristow D, Haynes JD, Sylvester R, Frith CD, Rees G (2005a) Blinking suppresses the neural response to unchanging retinal stimulation. Curr Biol 15:1296–1300.

Bristow D, Frith C, Rees G (2005b) Two distinct neural effects of blinking on human visual processing. Neuroimage 27:136–145.

Burlingham CS, Mirbagheri S, Heeger DJ (2022) A unified model of the task-evoked pupil response. Sci Adv 8:eabi9979.

Cantero JL, Atienza M, Madsen JR, Stickgold R (2004) Gamma EEG dynamics in neocortex and hippocampus during human wakefulness and sleep. Neuroimage 22:1271–1280.

Cardoso MMB, Lima B, Sirotin YB, Das A (2019) Task-related hemodynamic responses are modulated by reward and task engagement. PLoS Biol 17: e3000080.

Carter ME, Yizhar O, Chikahisa S, Nguyen H, Adamantidis A, Nishino S, Deisseroth K, de Lecea L (2010) Tuning arousal with optogenetic modulation of locus coeruleus neurons. Nat Neurosci 13:1526–1533.

Chang L, Breuninger T, Euler T (2013) Chromatic coding from cone-type unselective circuits in the mouse retina. Neuron 77:559–571.

Cirelli C (2009) The genetic and molecular regulation of sleep: from fruit flies to humans. Nat Rev Neurosci 10:549–560.

Drew P, Sayres R, Watanabe K, Shimojo S (2001) Pupillary response to chromatic flicker. Exp Brain Res 136:256–262.

Drew PJ, Feldman DE (2009) Intrinsic signal imaging of deprivation-induced contraction of whisker representations in rat somatosensory cortex. Cereb Cortex 19:331–348.

Drew PJ, Shih AY, Driscoll JD, Knutsen PM, Blinder P, Davalos D, Akassoglou K, Tsai PS, Kleinfeld D (2010) Chronic optical access through a polished and reinforced thinned skull. Nat Methods 7:981–984.

Drew PJ, Winder AT, Zhang Q (2019) Twitches, blinks, and fidgets: important generators of ongoing neural activity. Neuroscientist 25:298–313.

Drew PJ, Mateo C, Turner KL, Yu X, Kleinfeld D (2020) Ultra-slow oscillations in fMRI and resting-state connectivity: neuronal and vascular contributions and technical confounds. Neuron 107:782–804.

Echagarruga CT, Gheres KW, Norwood JN, Drew PJ (2020) nNOS-expressing interneurons control basal and behaviorally evoked arterial dilation in somatosensory cortex of mice. Elife 9:e60533.

Einhäuser W, Koch C, Carter OL (2010) Pupil dilation betrays the timing of decisions. Front Hum Neurosci 4:18.

Feng J, Zhang C, Lischinsky JE, Jing M, Zhou J, Wang H, Zhang Y, Dong A, Wu Z, Wu H, Chen W, Zhang P, Zou J, Hires SA, Zhu JJ, Cui G, Lin D, Du J, Li Y (2019) A genetically encoded fluorescent sensor for rapid and specific *in vivo* detection of norepinephrine. Neuron 102:745–761.e8.

Fultz NE, Bonmassar G, Setsompop K, Stickgold RA, Rosen BR, Polimeni JR, Lewis LD (2019) Coupled electrophysiological, hemodynamic, and cerebrospinal fluid oscillations in human sleep. Science 366:628–631.

Gao YR, Drew PJ (2014) Determination of vessel cross-sectional area by thresholding in Radon space. J Cereb Blood Flow Metab 34:1180–1187.

Gawne TJ, Martin JM (2000) Activity of primate V1 cortical neurons during blinks. J Neurophysiol 84:2691–2694.

Gilzenrat MS, Nieuwenhuis S, Jepma M, Cohen JD (2010) Pupil diameter tracks changes in control state predicted by the adaptive gain theory of locus coeruleus function. Cogn Affect Behav Neurosci 10:252–269.

Goadsby PJ, Lambert GA, Lance JW (1985) The mechanism of cerebrovascular vasoconstriction in response to locus coeruleus stimulation. Brain Res 326:213–217.

Golan T, Davidesco I, Meshulam M, Groppe DM, Megevand P, Yeagle EM, Goldfinger MS, Harel M, Melloni L, Schroeder CE, Deouell LY, Mehta AD, Malach R (2016) Human intracranial recordings link suppressed transients rather than 'filling-in' to perceptual continuity across blinks. Elife 5:e17243.

Gray SR, Ye L, Ye JY, Paukert M (2021) Noradrenergic terminal short-term potentiation enables modality-selective integration of sensory input and vigilance state. Sci Adv 7:eabk1378.

Guipponi O, Odouard S, Pinède S, Wardak C, Ben Hamed S (2015) fMRI cortical correlates of spontaneous eye blinks in the nonhuman primate. Cereb Cortex 25:2333–2345.

Hakerem G, Sutton S (1966) Pupillary response at visual threshold. Nature 212:485–486.

Hamel E (2006) Perivascular nerves and the regulation of cerebrovascular tone. J Appl Physiol (1985) 100:1059–1064.

Hayat H, Regev N, Matosevich N, Sales A, Paredes-Rodriguez E, Krom AJ, Bergman L, Li Y, Lavigne M, Kremer EJ, Yizhar O, Pickering AE, Nir Y (2020) Locus coeruleus norepinephrine activity mediates sensory-evoked awakenings from sleep. Sci Adv 6:eaaz4232.

Hess EH, Polt JM (1964) Pupil size in relation to mental activity during simple problem-solving. Science 143:1190–1192.

Holland MK, Tarlow G (1972) Blinking and mental load. Psychol Rep 31:119–127.

Huo BX, Smith JB, Drew PJ (2014) Neurovascular coupling and decoupling in the cortex during voluntary locomotion. J Neurosci 34:10975–10981.

Huo BX, Gao YR, Drew PJ (2015) Quantitative separation of arterial and venous cerebral blood volume increases during voluntary locomotion. Neuroimage 105:369–379.

Hupé JM, Bordier C, Dojat M (2012) A BOLD signature of eyeblinks in the visual cortex. Neuroimage 61:149–161.

Jing M, et al. (2020) An optimized acetylcholine sensor for monitoring *in vivo* cholinergic activity. Nat Methods 17:1139–1146.

Jones BE (2020) Arousal and sleep circuits. Neuropsychopharmacology 45:6–20.

Joshi S, Li Y, Kalwani RM, Gold JI (2016) Relationships between pupil diameter and neuronal activity in the locus coeruleus, colliculi, and cingulate cortex. Neuron 89:221–234.

Kahneman D, Beatty J (1966) Pupil diameter and load on memory. Science 154:1583–1585.

Kaminer J, Powers AS, Horn KG, Hui C, Evinger C (2011) Characterizing the spontaneous blink generator: an animal model. J Neurosci 31:11256–11267.

Karimi Abadchi J, Nazari-Ahangarkolaee M, Gattas S, Bermudez-Contreras E, Luczak A, McNaughton BL, Mohajerani MH (2020) Spatiotemporal patterns of neocortical activity around hippocampal sharp-wave ripples. Elife 9:e51972.

Karson CN (1979) Oculomotor signs in a psychiatric population: a preliminary report. Am J Psychiatry 136:1057–1060.

Karson CN (1983) Spontaneous eye-blink rates and dopaminergic systems. Brain 106 (Pt 3):643–653.

Karson CN, Dykman RA, Paige SR (1990) Blink rates in schizophrenia. Schizophr Bull 16:345–354.

Kedarasetti RT, Drew PJ, Costanzo F (2020a) Arterial pulsations drive oscillatory flow of CSF but not directional pumping. Sci Rep 10:10102.

Kedarasetti RT, Turner KL, Echagarruga C, Gluckman BJ, Drew PJ, Costanzo F (2020b) Functional hyperemia drives fluid exchange in the paravascular space. Fluids Barriers CNS 17:52.

Kedarasetti RT, Drew PJ, Costanzo F (2022) Arterial vasodilation drives convective fluid flow in the brain: a poroelastic model. Fluids Barriers CNS 19:34.

Kim JH, Jung AH, Jeong D, Choi I, Kim K, Shin S, Kim SJ, Lee SH (2016) Selectivity of neuromodulatory projections from the basal forebrain and locus ceruleus to primary sensory cortices. J Neurosci 36:5314–5327.

Kjaerby C, Andersen M, Hauglund N, Untiet V, Dall C, Sigurdsson B, Ding F, Feng J, Li Y, Weikop P, Hirase H, Nedergaard M (2022) Memory-enhancing properties of sleep depend on the oscillatory amplitude of norepinephrine. Nat Neurosci 25:1059–1070.

Kleinfeld D, Blinder P, Drew PJ, Driscoll JD, Muller A, Tsai PS, Shih AY (2011) A guide to delineate the logic of neurovascular signaling in the brain. Front Neuroenergetics 3:1.

Larsen RS, Waters J (2018) Neuromodulatory correlates of pupil dilation. Front Neural Circuits 12:21.

Le Van Quyen M, Staba R, Bragin A, Dickson C, Valderrama M, Fried I, Engel J (2010) Large-scale microelectrode recordings of high-frequency gamma oscillations in human cortex during sleep. J Neurosci 30:7770–7782.

Liu X, Yanagawa T, Leopold DA, Chang C, Ishida H, Fujii N, Duyn JH (2015) Arousal transitions in sleep, wakefulness, and anesthesia are characterized by an orderly sequence of cortical events. Neuroimage 116:222–231.

Liu X, de Zwart JA, Schölvinck ML, Chang C, Ye FQ, Leopold DA, Duyn JH (2018) Subcortical evidence for a contribution of arousal to fMRI studies of brain activity. Nat Commun 9:395.

Longden TA, Dabertrand F, Koide M, Gonzales AL, Tykocki NR, Brayden JE, Hill-Eubanks D, Nelson MT (2017) Capillary K(+)-sensing initiates retrograde hyperpolarization to increase local cerebral blood flow. Nat Neurosci 20:717–726.

Ma Y, Shaik MA, Kim SH, Kozberg MG, Thibodeaux DN, Zhao HT, Yu H, Hillman EM (2016a) Wide-field optical mapping of neural activity and brain haemodynamics: considerations and novel approaches. Philos Trans R Soc Lond B Biol Sci 371:20150360.

Ma Y, Shaik MA, Kozberg MG, Kim SH, Portes JP, Timerman D, Hillman EMC (2016b) Resting-state hemodynamics are spatiotemporally coupled to synchronized and symmetric neural activity in excitatory neurons. Proc Natl Acad Sci U S A 113:E8463–E8471.

Mathis A, Mamidanna P, Cury KM, Abe T, Murthy VN, Mathis MW, Bethge M (2018) DeepLabCut: markerless pose estimation of user-defined body parts with deep learning. Nat Neurosci 21:1281–1289.

McGinley MJ, David SV, McCormick DA (2015) Cortical membrane potential signature of optimal states for sensory signal detection. Neuron 87:179–192.

Megemont M, McBurney-Lin J, Yang H (2022) Pupil diameter is not an accurate real-time readout of locus coeruleus activity. Elife 11:e70510.

Mirg S, Chen H, Turner KL, Gheres KW, Liu J, Gluckman BJ, Drew PJ, Kothapalli SR (2022a) Awake mouse brain photoacoustic and optical imaging through a transparent ultrasound cranial window. Opt Lett 47:1121–1124.

Mirg S, Turner KL, Chen H, Drew PJ, Kothapalli SR (2022b) Photoacoustic imaging for microcirculation. Microcirculation 29:e12776.

Montgomery SM, Sirota A, Buzsáki G (2008) Theta and gamma coordination of hippocampal networks during waking and rapid eye movement sleep. J Neurosci 28:6731–6741.

Morad Y, Lemberg H, Yofe N, Dagan Y (2000) Pupillography as an objective indicator of fatigue. Curr Eye Res 21:535–542.

Murphy PR, O'Connell RG, O'Sullivan M, Robertson IH, Balsters JH (2014) Pupil diameter covaries with BOLD activity in human locus coeruleus. Hum Brain Mapp 35:4140–4154.

Musall S, Kaufman MT, Juavinett AL, Gluf S, Churchland AK (2019) Single-trial neural dynamics are dominated by richly varied movements. Nat Neurosci 22:1677–1686.

Nakamori K, Odawara M, Nakajima T, Mizutani T, Tsubota K (1997) Blinking is controlled primarily by ocular surface conditions. Am J Ophthalmol 124:24–30.

Nakano T, Kato M, Morito Y, Itoi S, Kitazawa S (2013) Blink-related momentary activation of the default mode network while viewing videos. Proc Natl Acad Sci U S A 110:702–706.

Nassar MR, Rumsey KM, Wilson RC, Parikh K, Heasly B, Gold JI (2012) Rational regulation of learning dynamics by pupil-linked arousal systems. Nat Neurosci 15:1040–1046.

Onorati F, Barbieri R, Mauri M, Russo V, Mainardi L (2013) Characterization of affective states by pupillary dynamics and autonomic correlates. Front Neuroeng 6:9.

Osorio-Forero A, Cardis R, Vantomme G, Guillaume-Gentil A, Katsioudi G, Devenoges C, Fernandez LMJ, Luthi A (2021) Noradrenergic circuit control of non-REM sleep substates. Curr Biol 31:5009–5023.e7.

Pais-Roldan P, Takahashi K, Sobczak F, Chen Y, Zhao X, Zeng H, Jiang Y, Yu X (2020) Indexing brain state-dependent pupil dynamics with simultaneous fMRI and optical fiber calcium recording. Proc Natl Acad Sci USA U S A 117:6875–6882.

Paukert M, Agarwal A, Cha J, Doze VA, Kang JU, Bergles DE (2014) Norepinephrine controls astroglial responsiveness to local circuit activity. Neuron 82:1263–1270.

Petersen CC (2007) The functional organization of the barrel cortex. Neuron 56:339–355.

Petersen CC (2014) Cortical control of whisker movement. Annu Rev Neurosci 37:183–203.

Pilorz V, Tam SKE, Hughes S, Pothecary CA, Jagannath A, Hankins MW, Bannerman DM, Lightman SL, Vyazovskiy VV, Nolan PM, Foster RG, Peirson SN (2016) Melanopsin regulates both sleep-promoting and arousal-promoting responses to light. PLoS Biol 14:e1002482.

Pisauro MA, Dhruv NT, Carandini M, Benucci A (2013) Fast hemodynamic responses in the visual cortex of the awake mouse. J Neurosci 33:18343–18351.

Pisauro MA, Benucci A, Carandini M (2016) Local and global contributions to hemodynamic activity in mouse cortex. J Neurophysiol 115:2931–2936.

Poe GR, Foote S, Eschenko O, Johansen JP, Bouret S, Aston-Jones G, Harley CW, Manahan-Vaughan D, Weinshenker D, Valentino R, Berridge C, Chandler DJ, Waterhouse B, Sara SJ (2020) Locus coeruleus: a new look at the blue spot. Nat Rev Neurosci 21:644–659.

Polack PO, Friedman J, Golshani P (2013) Cellular mechanisms of brain state-dependent gain modulation in visual cortex. Nat Neurosci 16:1331–1339.

Preuschoff K, 't Hart BM, Einhäuser W (2011) Pupil dilation signals surprise: evidence for noradrenaline's role in decision making. Front Neurosci 5:115.

Privitera M, Ferrari KD, von Ziegler LM, Sturman O, Duss SN, Floriou-Servou A, Germain P-L, Vermeiren Y, Wyss MT, De Deyn PP, Weber B, Bohacek J (2020) A complete pupillometry toolbox for real-time monitoring of locus coeruleus activity in rodents. Nat Protoc 15:2301–2320.

Raichle ME, Hartman BK, Eichling JO, Sharpe LG (1975) Central noradrenergic regulation of cerebral blood flow and vascular permeability. Proc Natl Acad Sci U S A 72:3726–3730.

Rasmussen R, Nicholas E, Petersen NC, Dietz AG, Xu Q, Sun Q, Nedergaard M (2019) Cortex-wide changes in extracellular potassium ions parallel brain state transitions in awake behaving mice. Cell Rep 28:1182–1194.e4.

Reimer J, Froudarakis E, Cadwell CR, Yatsenko D, Denfield GH, Tolias AS (2014) Pupil fluctuations track fast switching of cortical states during quiet wakefulness. Neuron 84:355–362.

Reimer J, McGinley MJ, Liu Y, Rodenkirch C, Wang Q, McCormick DA, Tolias AS (2016) Pupil fluctuations track rapid changes in adrenergic and cholinergic activity in cortex. Nat Commun 7:13289.

Salkoff DB, Zagha E, McCarthy E, McCormick DA (2020) Movement and performance explain widespread cortical activity in a visual detection task. Cereb Cortex 30:421–437.

Sánchez-López A, Escudero M (2011) Tonic and phasic components of eye movements during REM sleep in the rat. Eur J Neurosci 33:2129–2138.

Saper CB, Fuller PM (2017) Wake-sleep circuitry: an overview. Curr Opin Neurobiol 44:186–192.

Schwarz LA, Luo L (2015) Organization of the locus coeruleus-norepinephrine system. Curr Biol 25:R1051–R1056.

Senzai Y, Scanziani M (2022) A cognitive process occurring during sleep is revealed by rapid eye movements. Science 377:999–1004.

Shih AY, Mateo C, Drew PJ, Tsai PS, Kleinfeld D (2012) A polished and reinforced thinned-skull window for long-term imaging of the mouse brain. J Vis Exp 7:3742.

Siegle GJ, Ichikawa N, Steinhauer S (2008) Blink before and after you think: blinks occur prior to and following cognitive load indexed by pupillary responses. Psychophysiology 45:679–687.

Sirotin YB, Das A (2009) Anticipatory haemodynamic signals in sensory cortex not predicted by local neuronal activity. Nature 457:475–479.
Sobczak F, Pais-Roldán P, Takahashi K, Yu X (2021) Decoding the brain state-dependent relationship between pupil dynamics and resting state fMRI signal fluctuation. Elife 10:e68980.
Steriade M, Nunez A, Amzica F (1993) A novel slow (< 1 Hz) oscillation of neocortical neurons *in vivo*: depolarizing and hyperpolarizing components. J Neurosci 13:3252–3265.
Stern JA, Walrath LC, Goldstein R (1984) The endogenous eyeblink. Psychophysiology 21:22–33.
Stern JA, Boyer D, Schroeder D (1994) Blink rate: a possible measure of fatigue. Hum Factors 36:285–297.
Strauch C, Wang CA, Einhäuser W, Van der Stigchel S, Naber M (2022) Pupillometry as an integrated readout of distinct attentional networks. Trends Neurosci 45:635–647.
Stringer C, Pachitariu M, Steinmetz N, Reddy CB, Carandini M, Harris KD (2019) Spontaneous behaviors drive multidimensional, brainwide activity. Science 364:255.
Sullivan D, Mizuseki K, Sorgi A, Buzsaki G (2014) Comparison of sleep spindles and theta oscillations in the hippocampus. J Neurosci 34:662–674.
Tagliazucchi E, Laufs H (2014) Decoding wakefulness levels from typical fMRI resting-state data reveals reliable drifts between wakefulness and sleep. Neuron 82:695–708.
Toussay X, Basu K, Lacoste B, Hamel E (2013) Locus coeruleus stimulation recruits a broad cortical neuronal network and increases cortical perfusion. J Neurosci 33:3390–3401.
Tran CHT, Peringod G, Gordon GR (2018) Astrocytes integrate behavioral state and vascular signals during functional hyperemia. Neuron 100:1133–1148.e3.
Turner KL, Gheres KW, Proctor EA, Drew PJ (2020) Neurovascular coupling and bilateral connectivity during NREM and REM sleep. Elife 9:e62071.
Van Orden KF, Limbert W, Makeig S, Jung TP (2001) Eye activity correlates of workload during a visuospatial memory task. Hum Factors 43:111–121.
van Veluw SJ, Hou SS, Calvo-Rodriguez M, Arbel-Ornath M, Snyder AC, Frosch MP, Greenberg SM, Bacskai BJ (2020) Vasomotion as a driving force for paravascular clearance in the awake mouse brain. Neuron 105 105:549–561.e5.
Vazquez AL, Fukuda M, Crowley JC, Kim SG (2014) Neural and hemodynamic responses elicited by forelimb- and photo-stimulation in channelrhodopsin-2 mice: insights into the hemodynamic point spread function. Cereb Cortex 24:2908–2919.
Vinck M, Batista-Brito R, Knoblich U, Cardin JA (2015) Arousal and locomotion make distinct contributions to cortical activity patterns and visual encoding. Neuron 86:740–754.
Weber F, Dan Y (2016) Circuit-based interrogation of sleep control. Nature 538:51–59.
Winder AT, Echagarruga C, Zhang Q, Drew PJ (2017) Weak correlations between hemodynamic signals and ongoing neural activity during the resting state. Nat Neurosci 20:1761–1769.
Xie L, Kang H, Xu Q, Chen MJ, Liao Y, Thiyagarajan M, O'Donnell J, Christensen DJ, Nicholson C, Iliff JJ, Takano T, Deane R, Nedergaard M (2013) Sleep drives metabolite clearance from the adult brain. Science 342:373–377.
Yang H, Bari BA, Cohen JY, O'Connor DH (2021) Locus coeruleus spiking differently correlates with S1 cortex activity and pupil diameter in a tactile detection task. Elife 10:e64327.
Yoss RE, Moyer NJ, Hollenhorst RW (1970) Pupil size and spontaneous pupillary waves associated with alertness, drowsiness, and sleep. Neurology 20:545–554.
Yüzgeç Ö, Prsa M, Zimmermann R, Huber D (2018) Pupil size coupling to cortical states protects the stability of deep sleep via parasympathetic modulation. Curr Biol 28:392–400.e3.
Zhang Q, Roche M, Gheres KW, Chaigneau E, Kedarasetti RT, Haselden WD, Charpak S, Drew PJ (2019) Cerebral oxygenation during locomotion is modulated by respiration. Nat Commun 10:5515.
Zhang Q, Turner KL, Gheres KW, Hossain MS, Drew PJ (2022a) Behavioral and physiological monitoring for awake neurovascular coupling experiments: a how-to guide. Neurophoton 9:021905.
Zhang Q, Cramer SR, Ma Z, Turner KL, Gheres KW, Liu Y, Drew PJ, Zhang N (2022b) Brain-wide ongoing activity is responsible for significant cross-trial BOLD variability. Cereb Cortex 32:5311–5329.